Estimates of Biomass Yield for Perennial Bioenergy Grasses in the USA

Yang Song · Atul K. Jain · William Landuyt ·
Haroon S. Kheshgi · Madhu Khanna

Abstract Perennial grasses, such as switchgrass (*Panicum viragatum*) and Miscanthus (*Miscanthus × giganteus*), are potential choices for biomass feedstocks with low-input and high dry matter yield per hectare in the USA and Europe. However, the biophysical potential to grow bioenergy grasses varies with time and space due to changes in environmental conditions. Here, we integrate the dynamic crop growth processes for Miscanthus and two different cultivars of switchgrass, Cave-in-Rock and Alamo, into a land surface model, the Integrated Science Assessment Model (ISAM), to estimate the spatial and temporal variations of biomass yields over the period 2001–2012 in the eastern USA. The validation with observed data from sites across diverse environmental conditions suggests that the model is able to simulate the dynamic response of bioenergy grass growth to changes in environmental conditions in the central and south of the USA. The model is applied to identify four spatial zones characterized by their average yield amplitude and temporal yield variance (or stability) over 2001–2012 in the USA: a high and stable yield zone (HS), a high and unstable yield zone (HU), a low and stable yield zone (LS), and a low and unstable yield zone (LU). The HS zones are mainly distributed in the regions with precipitation larger than 600 mm, and mean temperature range 292–294 K during the growing season, including southern Missouri, north-western Arkansas, southern Illinois, southern Indiana, southern Ohio, western Kentucky, and parts of northern Virginia. The LU yield zones are distributed in southern parts of Great Plains with water stress conditions and higher temporal variances in precipitation, such as Oklahoma and Kansas. Three bioenergy grasses may not grow in the LS yield zones, including western parts of Great Plains due to extreme low precipitation and poor soil texture, and upper part of north central, northeastern, and northern New England due to extreme cold conditions.

Keywords Bioenergy grasses · Miscanthus · Switchgrass · Biomass yield · ISAM

Introduction

The USA is the largest producer of biofuels in the world and is converting nearly 40 % of its corn production into 14 billion gallons per year of corn ethanol. Further increases in biofuel production from cellulosic feedstocks are mandated by the Renewable Fuel Standard (RFS), established by the Energy Independence and Security Act, 2007, which mandates production of at least 16 billion gallons per year of cellulosic biofuels by 2022 [1].

Although conversion of cellulosic biomass to fuel is not yet commercially viable, considerable research is underway on high-yielding feedstock sources that could provide abundant biomass for large-scale cellulosic biofuel production. Among all non-grain feedstocks, two perennial crops, switchgrass (*Panicum viragatum*) and Miscanthus (*Miscanthus × giganteus*), have been identified as among the best choices

Y. Song · A. K. Jain (✉)
Department of Atmospheric Sciences, University of Illinois, Urbana, IL 61801, USA
e-mail: jain1@illinois.edu

W. Landuyt · H. S. Kheshgi
ExxonMobil Research and Engineering Company, Annandale, NJ 08801, USA

M. Khanna
Department of Agriculture and Consumer Economics, University of Illinois, Urbana, IL 61801, USA

for low-input and high dry matter yield per hectare in the USA and Europe [2–4]. Miscanthus is a C4 perennial rhizomatous grass. It has been extensively grown in Europe for over 20 years and is recently being grown in field trials in the USA [3]. Switchgrass is also a C4 native warm-season grass from the USA and has historically been used as forage. Studies suggest that latitude-of-origin of different bioenergy grasses determines their varied adaptability to edaphic conditions, such as winter hardiness, day length, heat, dry and cold conditions, etc. [5]. Miscanthus × giganteus is more adapt to the region below the US plant hardiness zone (PHZ) 5 [6]. On the other hand, switchgrass cultivars are usually divided into upland and lowland. Upland cultivars, such as Cave-in-Rock, are more adapted to middle and northern latitudes (PHZ 4–PHZ 7). Lowland cultivars, such as Alamo, grow better in lower latitudes (PHZ 6–PHZ 9) [7, 8]. The detailed physiological differences between upland and lowland switchgrasses, as well as their differences with Miscanthus, have been discussed in previous studies [4, 8].

While these perennial grasses have potential to help meet future energy demand, the extent to which this potential can be realized will depend on the biophysical potential to grow these grasses while minimizing the diversion of land from food production. We evaluate this potential by assessing the productivity of these perennial grasses under different environmental conditions in the USA. A number of crop productivity modeling studies have estimated the biomass yields for Miscanthus and switchgrass in the USA. For example, Jager et al. [9] have developed empirical models to estimate yield from factors associated with climate, soils, and management for both lowland and upland switchgrass cultivars. However, these model estimates are usually limited by available observation data from field trials and have limited representation of diverse climate, soil, and topographical conditions across the USA [10]. No attempt has been made to evaluate the biomass yield for Miscanthus using an empirical-based approach, mainly because field trials for Miscanthus are sparser than for switchgrass and usually centralized in the Midwest region [3, 11]. Several attempts have therefore been made using mechanistic models to estimate the yield and the spatial and temporal variability in yield of bioenergy grasses, including ALMANAC [12], MISCANMOD [13, 14], MISCANFOR [15], EPIC [16], WIMOVAC (BIOCRO) [17], Agro-IBIS [18], Agro-BGC [19], and TEM [20]. Nair et al. [10] reviewed the differences among these models. According to Nair et al. [10], the ALMANAC, MISCANMOD, MISCANFOR, and EPIC models use relatively simple radiation use efficiency method to simulate the biomass yields, while other models use a more mechanistic biophysical approach to simulate the carbon uptake and assimilation rates. Partitioning of carbon among leaves, stem, root, and rhizome pools are based on fixed carbon allocation fraction at each phenology stage. WIMOVAC (BIOCRO) only accounts for the water limitation on biomass allocation, whereas the ALMANC and EPIC models not only account for water limitation effect on biomass allocation but also temperature, nitrogen, and aeration limitations on plant phenology and biomass yield. Moreover, ALMANC and EPIC are the only two models that account for full hydrological cycle processes. Nitrogen cycle dynamics processes are only considered in the EPIC, ALMANAC, and Agro-BGC models.

This study builds upon and extends the approaches of the models discussed above and aims to integrate the dynamic crop growth processes for Miscanthus and two cultivars of switchgrass perennial grasses into a land surface model, the Integrated Science Assessment Model (ISAM), to estimate the biomass yields for these three grasses in the USA. The western USA, where bioenergy grasses could not survive due to drier conditions [7], is excluded in this study (irrigation is not addressed in this study). The adaptability of three bioenergy grasses at different latitudes is determined by accounting various environmental factors, which vary with day length, the effect of soil texture, soil slope, bedrock layer depth on water uptake by the grasses, and tolerance to winter hardiness, heat, dry, and cold conditions.

While ISAM methodologies to model carbon assimilation, water and energy fluxes, and carbon and nitrogen dynamics for various plant functional types have been described elsewhere [21–25], this study extends ISAM model by accounting additional dynamic structural properties of vegetation, which are specific to the perennial bioenergy grasses. These include the following: (1) a specific phenology development scheme and its variation with latitude, which is controlled by thermal, photoperiod, and extreme meteorological conditions (e.g., frost and drought); (2) a dynamic carbon allocation process to allocate assimilated carbon among root, rhizome, leaf, and stem based on resource availability (e.g., light, water, and nutrient); (3) parameterization of N resorption rate; (4) parameterization of leaf area index (LAI) growth process, which is sensitive to photoperiod.

The objectives of this study are to (1) calibrate and validate different parameters of the above parameterization schemes for three perennial grasses: Miscanthus and two switchgrass cultivars, Cave-in-Rock and Alamo; (2) evaluate ISAM-calculated carbon assimilation rate, LAI, and aboveground/belowground biomass yields for three energy crops using observational data; (3) estimate spatial and temporal biomass yield patterns for the period 2001–2012 in the USA; and (4) compare ISAM-estimated biomass yields with other published studies.

Methods

Model Description

ISAM is a land surface model, which coupled biogeochemical (carbon and nitrogen) module [25] and biogeophysical (energy and hydrology) module [26, 27]. The model calculates carbon, nitrogen, energy, and water fluxes at $0.5 \times 0.5°$ spatial resolution and at multiple temporal resolutions ranging from half-hour to yearly time steps. The details about the model structure, parameterization, and performance have been introduced in previous studies [21–25]. In the following, we provide the details of the processes added to the model, which are specific for this study.

Model Extension

The formulations for dynamic growth processes considered for bioenergy grasses—such as allocation of assimilated carbon among above- and belowground vegetation pools and development of vegetation structure (*LAI*, canopy height and root depth), etc.—are the same as for the row crops described by Song et al. [24]; here, we describe the calibration of model parameters and model validation, specific to the model of energy grasses. However, the phenology for bioenergy grasses is different than row crops and is described in "Phenology Development". In addition, we added a rhizome pool and implemented the carbon reallocation between root and rhizome for the bioenergy grasses (Carbon Allocation). The parameterization of N resorption and the sensitivity of LAI growth to photoperiod are also considered (Parameterization of N Resorption Rate for Bioenergy Grasses and LAI Calculation). In the following, we described dynamic processes that had been implemented in ISAM for the current study.

Phenology Development

Miscanthus is planted through rhizomes and switchgrasses through seeds. During the growing season, phenology is divided into five stages: emergence period, initial vegetative period, normal vegetative period, initial reproductive period, and post reproductive period (Fig. 1). After post reproductive period, bioenergy grasses go to the winter dormancy stage, which lasts until the rhizomes emerge next year. The grasses are harvested each year at the beginning of winter dormancy time.

The planting date for Miscanthus rhizomes is determined based on the shallow soil layers' temperature and air temperature [24]. The seeding dates for switchgrass are determined by both soil and surface air thermal conditions and accumulated precipitation over a week time just prior to the planting date. Since switchgrasses may not adapt to the region in the west of the 100th meridian [7], and Miscanthus may have difficulty to survive in the region with less than 0.75 m of annual accumulated precipitation [28], we exclude those regions which experience such environmental conditions—viz. the western USA. Switchgrass seeds are planted when the accumulated precipitation over the previous week is greater than the grass-specific minimum precipitation requirement (P_{crit}) [29] (Table 8). Each year after planting bioenergy grasses, the transitions of the different phenology stages are determined by thermal conditions and other factors, which are dependent on latitude of each grid cell [8, 30].

The thermal condition for each grid cell is expressed as the heat unit index above 0 °C (HUI0) (Eq. 1).

$$HUI0 = \frac{GDD0}{GDD0_{max}} \tag{1}$$

Here, GDD0 is the accumulated growing degree days above 0 °C summed from the first day of the year to the current day. $GDD0_{max}$ is the yearly summation of growing degree days above 0 °C averaged for the past 33 years (1980–2012), which represents the climatological thermal conditions [31]. The threshold values of HUI0 for classifying five phenology stages are listed in Table 8. The total number of days during each phenology stage does not exceed the maximum number of growing days of each phenology stage (D), as prescribed in the Table 8.

Latitudinal variability in the onset of the emergence stage and the initial reproductive stage (flowering time) is controlled by the photoperiod [5], which is expressed as the total day length and civil twilight of each day (L_{day}) in terms of hours. The onset of the emergence stage begins when the photoperiod value is above the critical photoperiod value for emergence (L_e). At the same time, the past week mean daily air temperature is above the base temperature (T_{base}) and soil temperature is above the critical emergence soil temperature (T_{soil_crit}). The values for T_{base} and T_{soil_crit} vary with bioenergy grasses due to their difference in tolerance to temperature (Table 8). The value for L_e varies with the origin of each bioenergy grass (Table 8). Alamo, which is originally from central Texas, can emerge at much shorter photoperiod than that for Cave-in-Rock and Miscanthus, which originally grew in southern Illinois [8]. In addition, the regression analyses of bioenergy grass yields on photoperiod [5, 32] indicate that growing Miscanthus and Cave-in-Rock in the south of its origin (Southern Illinois) will flower earlier due to exposure to shorter than normal day length in the summer, while growing Alamo switchgrass north of its origin (Central Texas) will cause it to flower late due to exposure to longer than normal day length in the summer. To parameterize this effect, the onset of the initial reproductive stage is initialized when the following two conditions are satisfied: (1) the estimated photoperiod value is less than the grass-specific critical photoperiod value for flowering (L_f), which is 13 h for Miscanthus and
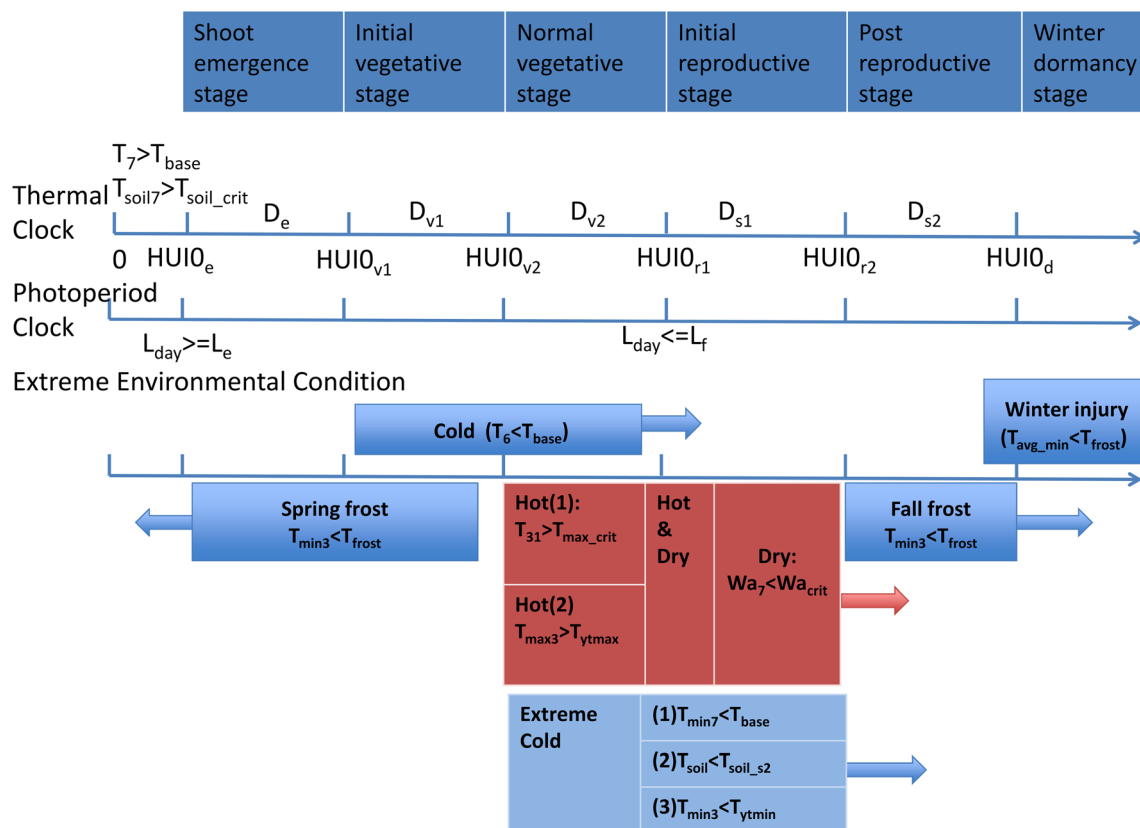
Fig. 1 The phenology scheme for bioenergy perennial grasses. The description of each variable is provided in the Table 8

Cave-in-Rock, but 12 h for Alamo [33–35]; (2) the minimum heat required for flowering (GDD_{v1}), which is expressed as the GDD above T_{base} from emergence to flowing time. Here GDD_{v1} is defined as a function of latitude (Eq. A1). The function is attained through regressing observed GDD_{v1} values from available sites with the latitude values of corresponding observation sites [36, 37]. If above two conditions are not satisfied, the initial reproductive stage can also be initiated when LAI values reach the grass-specific maximum LAI values (LAI_{max}) (Table 8).

Besides the normal phenology development, extreme environmental conditions can speed up or slow down the development of different phenology stages (Fig. 1). For example, spring frost can delay the onset of initial vegetative stage, whereas fall frost can trigger the earlier onset of the dormancy stage.

Alamo has been reported to be high heat tolerant, but sensitive to extreme cold and dry conditions [32, 38]. In contrast, Miscanthus is more sensitive to extreme hot and dry conditions than Cave-in-Rock and Alamo. Relative to Miscanthus and Alamo, Cave-in-Rock has higher cold and drought tolerances [32]. In addition, Moser and Vogel [39] suggest that warm-season grass species generally do not move more than 500 km north of their origin due to potential stand and rhizomes losses from over-winter injury. Calser [7] reports that Cave-in-Rock will have difficulty surviving in the

regions above the PHZ 3, whereas the survival rates of Alamo in the region above the PHZ 6 are low. Heaton et al. [40] finds that Miscanthus is able to survive with −20 °C of air temperature and −6 °C of soil temperature in Illinois, but experiences 90 % of loss in Wisconsin. Past field experiments have failed to establish Miscanthus in the PHZ 3 and PHZ 4 [personal communication with M. Casler].

ISAM accounts for sensitivity of bioenergy grasses to extreme cold, dry, or hot conditions, as discussed above. The spring and fall frost are triggered when previous 3 days average daily minimum temperature (T_{min3}) is less than the grass-specific critical air minimum temperature for frost (T_{frost}). Extreme cold conditions, expressed as previous 6 days (T_6) average daily temperature below T_{base}, during the initial vegetative stage can force the transition from the initial vegetative stage to the initial reproductive stage. Extreme cold weather conditions during the normal vegetative and the initial reproductive stages can induce the onset of the post reproductive stage with initiation of plant senescence [31]. Cold weather conditions are triggered when any of the following conditions are satisfied (Fig. 1): (1) the daily minimum temperature averaged for previous week (T_{min7}) is less than T_{base}; (2) the T_{min3} is less than the annual minimum temperature averaged for 1980–2012 (T_{ytmin}); (3) the daily soil temperature of root zone is less than the critical temperature for root zone (T_{soil_s2}). Extreme hot and dry conditions can also make the transition to

the post reproductive stage earlier without flowering [37]. Extreme hot conditions are triggered when one of the following conditions is met: (1) the mean daily temperature averaged for the last month is larger than the grass-specific maximum temperature ($T_{\mathrm{max\_crit}}$); (2) the previous 3 days average daily maximum temperature (T_{max3}) is larger than the annual maximum temperature averaged for 1980–2012 (T_{ytmax}). Dry conditions are activated when the daily mean soil water availability for previous week (Wa_7) is below the critical values of water availability for initiation of dry condition (Wa_{crit}). Here, soil water availability (Wa) is the weighted summation of water availability over the total number of soil layers (Eq. A2). The Wa is expressed as an index ranging from 0 to 1, which depends on the combined effects of precipitation, topography, soil texture, root depth, and its distribution in soil layers. The closer that Wa is to 1, the more soil water is available for grass growth. If extreme hot and dry conditions are met simultaneously, onset of the post reproductive stage is triggered. The over-winter injury is triggered when the average annual extreme minimum temperature ($T_{\mathrm{avg\_min}}$) is less than T_{frost}. The values for T_{frost}, T_{base}, T_{ytmin}, $T_{\mathrm{soil\_s2}}$, $T_{\mathrm{max\_crit}}$, T_{ytmax}, and Wa_7 (Table 8) are grass specific. Cave-in-Rock is parameterized with lower T_{frost}, $T_{\mathrm{soil\_s2}}$, and Wa_7 than that for Miscanthus and Alamo due to high tolerance to cold and dry condition, whereas Alamo is parameterized with higher $T_{\mathrm{max\_crit}}$ *than Miscanthus and Cave-in-Rock due to its high tolerance to hot condition.*

Carbon Allocation

Besides leaves, stem, roots, and production (seeds or flowers) carbon pools, here we added rhizome pool, which store carbon and nitrogen for the perennial growth. The emergence from rhizome and the carbon allocation among leaves, stems, roots, production, and rhizome are introduced as follows.

The amount of carbon in switchgrass seeds during germination is simulated as a function of seed weight and hydro and thermal conditions (Eqs. A3–A5) [41]. The carbon stored in switchgrasses seeds during the germination is allocated to root and leaf pools to build the root and initiate leaf development (Eq. A6). In the establishment year, the growing season starts with the germination of the seed. In the spring of the following years, the growing season starts with the emergence of rhizome. During the emergence of rhizomes, a fraction of rhizome carbon is allocated to leaf, stem, and root pools according to Eq. A7. After the emergence stage, leaves start assimilating carbon and the assimilated carbon is allocated to stem and root, as well as production pools. The amounts of the carbon allocation fractions at each model time step are determined dynamically based on the availability of water, light, and nitrogen as described in Song et al. [24].

Initial carbon allocation fractions to leaf (*Al*), stem (*As*), root (*Ar*), and rhizome (*Arh_r*) during each phenology stage (Table 8) are parameterized based on different growth requirements of canopy, stem, root, flowers, seeds, and rhizomes at each phenology stage. The canopy needs to be developed during the initial vegetative stage by keeping a large fraction of leaf-assimilated carbon in the leaf pool, but transferring a small fraction of leaf-assimilated carbon into root and stem. During the normal vegetative stage, the stem is elongated through increasing the fraction of assimilated carbon that allocates to stem. During the initial and post reproductive stages, leaf-assimilated carbon is transferred entirely to production and root pools to develop flowers and roots. Rhizomes grow over time through reallocation of a part of the root carbon pool to the rhizome pool. The reallocation fractions from root to rhizome are dynamically adjusted as a function of Wa (Eq. A8). In order to elongate the root to acquire more water under water stress conditions, the reallocation carbon fractions from root to rhizome pool are reduced according to Eq. A8. During the post reproductive stage, seed is produced for switchgrasses through increasing the fraction of leaf-assimilated carbon given to production pools. However, no carbon is allocated to production pools for Miscanthus, which has no seed production. Finally, the dynamic carbon allocation factor for each vegetation pool is modified by examining whether the minimum belowground/aboveground ratio (RS_{min}) is sufficient to maintain the structure of each grass. If this condition is not satisfied, all new assimilated carbon is allocated to root and rhizome. The senescence process follows the initiation of flowering. The leaf, stem, root, and rhizome senesce at fixed turnover rates (rlt_{leaf}, rlt_{stem}, rlt_{root}, rlt_{rhizome}) (Table 8), while leaf loss can be intensified due to dry or cold conditions. If the spring frost damage is triggered, the mortality of rhizomes, roots, and aboveground biomass increases linearly according to the Eqs. A9–A10. The fraction of rhizome mortality due to over-winter injury is assumed to be an exponential function of latitude (Eq. A11). The function is developed by regressing the reported values of standing/rhizome fraction loss [5, 42] on $T_{\mathrm{avg\_min}}$.

Parameterization of N Resorption Rate for Bioenergy Grasses

Temperate perennial grasses can mobilize N from actively growing tissues to rhizomes in response to winter or dry conditions [43]. This N can be reallocated to actively growing tissues in the following year and thus is important to maintain long-term N availability for growth of bioenergy grasses. N resorption for natural vegetation has been implemented in N cycle process in ISAM and the N availability on carbon assimilation is parameterized by linearly adjusting potential maximum carboxylation rate (V_{max}) with N availability [21, 22, 25]. Here, we parameterized N resorption rate (R_{cyc}) for bioenergy grasses based on measured seasonal variability in standing N and biomass for Miscanthus and Cave-in-Rock at Urbana, IL, site [43] (Table 8). It is assumed that R_{cyc} is

uniform across the different region and Alamo has the same R_{cyc} value as Cave-in-Rock in this study.

LAI Calculation

LAI is calculated as a function of leaf carbon and specific leaf area (SLA, defined as a ration of leaf area to leaf biomass). SLA for bioenergy grasses can vary with photoperiod. According to Van Esbroeck et al. [34], variation of leaf area with photoperiod differs among switchgrass cultivars. They found that the leaf size and number for Cave-in-Rock increased when the photoperiod increased from 12 to 16 h, but the reverse was true for Alamo. These results indicate that SLA for the northern cultivar (Cave-in-Rock) decreases from north to south due to exposure to shorter than normal day length in the summer, while SLA for southern cultivar (Alamo) decreases from south to north due to exposure to longer than normal day length in the summer. To parameterize photoperiod-sensitive SLA, we take the SLA in the natural origin of each cultivar (SLA_0) (Table 8) as a reference value and calculate SLA at each grid cell as a function of day length during the vegetative stage according to Eq. A12. It is assumed that the function between SLA and day length for Miscanthus is the same as that for Cave-in-Rock in this study.

Model Calibration and Evaluation Using Data from Various Sites

Description of Sites and Database

The field observation data for Miscanthus and Cave-in-Rock and Alamo switchgrasses from three sites in the USA were used to calibrate the model (Table 1). The choice of these sites for calibrations was due to the availability of the comprehensive observation data sets to calibrate the model parameters and processes. The Champaign-Urbana site 1 (CU1) for Miscanthus represents the earliest Miscanthus-growing region in the USA, whereas the CU2 site and Temple, TX (TE), site are at Cave-in-Rock's and Alamo's origin. The detailed soil and climatic characteristics as well as data available for different variables for each site are listed in Table 1.

The yield data collected at 17 Miscanthus planting sites (M1–M17), 28 Cave-in-Rock planting sites (C1–C28), and 22 Alamo planting sites (A1–A22) (Table 10) were used to evaluate the model performance in diverse environmental conditions. This measurement database aims to include available field experiments that could represent diverse environmental conditions and different geographical region. Field experiments with more than one time of harvest frequency per year and/or irrigation are excluded in this database, since current model has not considered these management practices. This database covers a large geospatial area of the USA, ranging from 26.68°N to 41.17°N for Miscanthus, from 26.22°N to 46.88°N for Cave-in-Rock switchgrass, and from 26.22°N to 39.62°N for Alamo switchgrass (Fig. 3). The soil texture and climatic characteristics are quite diverse at evaluated sites (Table 10). The annual mean air temperature during study years varies along the latitude gradient from 8 °C at the most northern site (Mandan, ND) to 24.5 °C at the most southern site (Weslaco, TX). The validation sites for Miscanthus cover five PHZs (PHZ 5–10a) with an average minimum air temperature of −28.9 to 1.7 °C. The validation sites for Cave-in-Rock include more northern PHZs ranging from PHZ 4a to PHZ 9b, with an average minimum temperature of −34.4 to −1.1 °C. Field experiments usually fail to establish Alamo switchgrass from PHZ 1a–5b due to extreme cold winter condition [personal communication with M. Casler]; thus, the validation sites for Alamo switchgrass only cover the region from PHZ 6a to 9b. The annual total precipitation follows the distinct longitude pattern with relatively less precipitation at the western sites and relative more precipitation at the eastern sites (Table 10). At most of validation sites have made efforts to mitigate the edge effect through excluding sampling from the edge of the plot, adjusting alley width, subsample size, planting density, harvest length, etc. [32, 37]. Detailed management information, such as planting time, seedling/rhizome planting weights, harvest frequency and time, fertilizer and irrigation, etc., were collected from references listed in Table 10.

Model Calibration

Hourly climate data for mean surface air temperature, precipitation rate, the incoming shortwave radiation, long-wave radiation, wind speed, and specific humidity are taken from North American Land Data Assimilation System (NLDAS-2) climate database (0.5×0.5°) [44]. Soil texture data is taken from the State Soil Geographic Database (STATSGO2) [45]. Both of these are used to drive the model simulation for each calibrated and validated site at an hourly time step. We start the modeling calculations for each site by prescribing current land cover distribution and atmospheric CO_2 concentrations of 369 ppm, representative of approximate condition in 2000, to allow soil water and soil temperature to reach an initial steady state, which takes approximately 200 years of model runs. Then, we assume that each site is fully covered with the corresponding bioenergy grasses (Miscanthus/Cave-in-rock Rock/Alamo) and run the model based on site-specific planting time, seed weight, and harvest time for each site [40, 46–49].

Table 1 The location of the calibrated site, its soil and climate characteristics, and a list of available data that are used to calibrate the model

Calibrated sites	Miscanthus	Cave-in-Rock	Alamo
Location	Urbana, IL (CU1) 40°03′N, 88°12′W	Urbana, IL (CU2) 40°02′N, 88°14′W	Temple, TX (TE) 31°04′N, 97°13′W
Plot area (ha)	0.20	0.010	0.014
Soil characteristics	Drummer/Flanagan series (fine-silty, mixed, mesic Typic Endoaquoll) Soil characteristics	Drummer/Flanagan series (fine-silty, mixed, mesic Typic Endoaquoll)	Houston black clay
Climate characteristics			
Annual temperature (°C)[a]	12	12	21
Annual accumulated precipitation (mm)[a]	1,021	1,021	895
Planting time (year)	2005	2002	1992
Available data	Daily gross leaf carbon assimilation rate (A) for period 2007–2008	Hourly gross leaf carbon assimilate rate (A) for period 2005–2006	Daily net leaf carbon assimilation rate (An) for period 1995–1997
	LAI for period 2007–2008	LAI for period 2005–2006	LAI for period 1995–1997
	Aboveground biomass for period 2005–2007	Mean aboveground biomass for period 2006–2008	Aboveground biomass for period 1995–1997
		Mean root biomass for period 2006–2008	Root biomass for period 1995–1997
		Mean rhizome biomass for period 2006–2008	
Source	[46]	[3, 47, 48]	[49]

[a] Annual temperature and annual accumulated precipitation are averaged over multiple measured years

The model parameters are calibrated and validated by minimizing the total sum of the squares of the difference between simulated and observed data for each bioenergy grass at each calibrated site [24]. The calibrated processes and corresponding parameters are listed in the Table 2.

Best Fit Model Results for Carbon Assimilation, LAI, and Above- and Belowground Biomass

We use the refined Willmott's index (dr) [50] to quantify the degree to which observed carbon assimilation rates, LAI, and biomass (aboveground, root, and rhizome biomass) are captured by the model. The dr is calculated as Eq. 2 and varies from −1 to 1. The value of 1 indicates perfect agreement between the modeled and observed values, while a dr of −1 indicates either lack of agreement between the model and observation or insufficient variation in observations to adequately test the model. The dr is calculated as:

$$
dr = \begin{cases} 1-\sum_{i=1}^{N}|P_i-O_i|/2\sum_{i=1}^{N}\left|O_i-\bar{O}\right| & if \ \sum_{i=1}^{N}|P_i-O_i| \leq 2\sum_{i=1}^{N}\left|O_i-\bar{O}\right| \\ 2\sum_{i=0}^{N}\left|O_i-\bar{O}\right|/\sum_{i=1}^{N}|P_i-O_i|-1 & if \ \sum_{i=1}^{N}|P_i-O_i| > 2\sum_{i=1}^{N}\left|O_i-\bar{O}\right| \end{cases}
$$

$$(2)$$

Here, P_i and O_i are the individual modeled and observed data, respectively. $\bar{O}$ is the mean of observed values. N is the number of the paired observed and modeled data. Based on the availability of observed carbon assimilation rate, we compare modeled with measured gross carbon assimilate rates (A) for Miscanthus and Cave-in-Rock as well as modeled with measured net carbon assimilation rate (An=A-leaf respiration) for Alamo switchgrass.

The dr values for A/An vary between 0.73 and 0.76 (Table 3), indicating that the model is able to capture the measured variations in carbon assimilation rates for all grasses. Modeled and measured carbon assimilation rates compare favorably across different growing seasons (Fig. 2a–c). The measured data is only available for Cave-in-Rock, and the comparisons between the modeled and measured hourly gross carbon assimilation rates for Cave-in-Rock at canopy level show close agreement (dr=0.75) (Figure S1), suggesting that the model is not only able to capture the daily assimilation rates for energy grasses but also the measured diurnal variability in carbon assimilation. The model also captures the seasonal development of LAI and its inter-annual variability for each three of energy grasses (Fig. 2d–f). The dr values calculated with all available data for three grasses vary between 0.78 and 0.90 (Table 3).

The modeled aboveground biomass production across two Miscanthus-growing seasons and three Alamo-growing seasons is in good agreement with the measured intra-annual and inter-annual variations (Fig. 2h, j), with an exception for a slight underestimation of peak biomass for Miscanthus at the CU1 site. The dr values are 0.83 and 0.87 for Miscanthus and Alamo grasses (Table 2). Because of the unavailability of the measured data for Miscanthus, we have not compared the modeled belowground biomass results with measurements. More importantly, the modeled root biomass for Alamo grass at the end of two continuous growing seasons is close to measured values (Fig. 2j), indicating that the model is able to predict continuous root growth across multiple years for Alamo grass. The model also accurately predicts the mean biomass partitioning among aboveground biomass, root, and rhizome across three continuous years for Cave-in-Rock (Fig. 2i). The relatively low dr values of 0.54 for root and 0.51 for rhizome are attributed to the overestimations of root and rhizome biomass at the end of growing season. These overestimations are due to the overestimation of carbon allocation to belowground pools at the end of growing season, when the minimum belowground/aboveground ratio (RS_{min}) is not satisfied to maintain the grass structure and thus model allocates all assimilated carbon to root and rhizome. This happens due to the uncertainty in parameterization of RS_{min}, which is attained in this study based on the measurement of a greenhouse experiment [51] and is assumed that its value does not vary spatially. However, the modeled root and rhizome biomass values still fall within the maximum measured uncertainty range values (Fig. 2i). Overall, the calibrated model is able to capture the diurnal and daily carbon assimilation rate and intra-annual and inter-annual variation in LAI and biomass production.

Model Evaluation

We evaluate model performance for estimated yields for each bioenergy grass across all evaluation sites discussed in Description of Sites and Database. First, the modeled and observed multi-year yields are averaged over the measured years to calculate the modeled and observed mean yield for each evaluation site. Then, the degrees to which observed mean yield across all sites are captured by modeled values are quantified by dr as discussed in Best Fit Model Results for Carbon Assimilation, LAI, and Above- and Belowground Biomass. The averaged tendency of the modeled yields relative to measured yields for each site is evaluated by calculating percent bias (PBIAS) (Eq. 3) [52]. Here, Y_i^o and Y_i^m are the modeled and measured yearly yields for the year i at each site. N is numbers of available data for each site. The closer the value of PBIAS is to zero, the higher the accuracy of the model results is and

Table 2 Calibrated parameter values for individual process. The three calibrated parameter values separated by comma (,) are for Miscanthus, Cave-in-Rock, and Alamo

Calibrated process	Equations	Calibrated parameters	Calibrated parameters values
Carbon assimilation	Ball-Berry equation	m	8, 3, 3
		b	0.03, 0.03, 0.03 [mol m^{-2} s^{-1}]
Phenology simulation	Eqs. A3–A7 in Song et al. [24]	$HUI0_e$	0.10, 0.10, 0.10
		$HUI0_{v1}$	0.12, 0.14, 0.14
		$HUI0_{v2}$	0.30, 0.35, 0.22
		$HUI0_{s1}$	0.66, 0.66, 0.41
		$HUI0_{s2}$	0.78, 0.73, 0.73
		$HUI0_d$	1.0, 1.0, 1.0
		D_e	8, 10, 10 [days]
		D_{v1}	50, 50, 50 [days]
		D_{v2}	60, 50, 60 [days]
		D_{s1}	60, 50, 50 [days]
		D_{s2}	76, 56, 76 [days]
Leaf carbon allocation and growth process	Eqs. A4–6 in this study and Eqs. A22 in Song et al. [24]	Al_{e1}	–, 0.30, 0.30
		Al_{e2}	0.45, 0.60, 0.6
		Al_{v1}	0.44, 0.50, 0.50
		Al_{v2}	0.20, 0.30, 0.30
		Al_{r1}	0, 0, 0
		Al_{r2}	0, 0, 0
Leaf senescence process	Eq. A39 in Song et al. [24]	kl_{r1}	0.035, 0.03, 0.03
		kl_{r2}	1.0, 1.0, 1.0
		RW_{max}	0.91, 1.0, 1.0
Stem, root, rhizome and seed carbon allocation process	Eqs. A4-6 in this study and Eqs. A22 in Song et al. [24]	As_{e1}	–, 0, 0
		Ar_{e1}	–, 0.70, 0.70
		Ah_{e1}	−0.02, −0.02, −0.01
		As_{e2}	0.25, 0.30, 0.30
		Ar_{e2}	0.30, 0.10, 0.10
		As_{v1}	0.20, 0.20, 0.20
		Ar_{v1}	0.36, 0.30, 0.30
		As_{v2}	0.60, 0.50, 0.60
		Ar_{v2}	0.20, 0.20, 0.10
		Arh_r_{v2}	0.30, 0.30, 0.30
		As_{r1}	0.15, 0.10, 0.10
		Ap_{r1}	0.20, 0.40, 0.40
		Ar_{r1}	0.65, 0.50, 0.50
		Arh_r_{r1}	0.50, 0.50, 0.50
		As_{r2}	0, 0, 0
		Ap_{r2}	0, 0.40, 0.40
		Ar_{r2}	1.0, 0.60, 0.60
		Arh_r_{r2}	0.50, 0.50, 0.50

the smaller the bias in the model results is. Positive PBIAS indicates the model underestimates the yield, and negative PBIAS indicates that the model overestimates the yield. The standard deviations (SD) from the mean for modeled and measured yields are calculated for each site using Eq. 4. Here, Y_i is the yearly yield for the year i and $\overline{Y}$ is the mean yield over N numbers of measured years for each site. The ± SD in mean yield represents the range of modeled and measured yields at each site. The comparison between modeled and observed SDs determines whether the model is able to capture the yearly yield variability at each site.

Table 3 The calculated Willmott index, dr, for various variables of Miscanthus, Cave-in-Rock, and Alamo

Variable	Bioenergy grass	n^a	dr
Assimilation Rate (A/An)[b]	Miscanthus	29	0.76
	Cave-in-Rock	110	0.74
	Alamo	29	0.73
LAI	Miscanthus	25	0.78
	Cave-in-Rock	24	0.90
	Alamo	17	0.87
Aboveground biomass	Miscanthus	30	0.83
	Cave-in-Rock	5	0.82
	Alamo	15	0.87
Root biomass	Miscanthus	–	–
	Cave-in-Rock	5	0.54
	Alamo	2	0.82
Rhizome biomass	Miscanthus	–	–
	Cave-in-Rock	5	0.51
	Alamo	–	–

[a] n is the total number of available data used to calculate dr

[b] A is gross carbon assimilation rate at Urbana, IL site for Miscanthus (CU1) and Cave-in-Rock (CU2). An is net carbon assimilation rate at Temple, TX, site (TE) for Alamo

$$PBIAS = \frac{\sum_{i=1}^{N} \left(Y_i^o - Y_i^m\right)}{\sum_{i=1}^{N} Y_i^o} \times 100\% \qquad (3)$$

$$SD = \sqrt{\frac{\sum_{i=1}^{N} \left(Y_i - \overline{Y}\right)^2}{N-1}} \qquad (4)$$

Evaluation of Model Estimated Yields

Overall, the modeled yields for Miscanthus, Cave-in-Rock, and Alamo are in good agreement with measured yields at evaluation sites, with *dr* values of 0.87, 0.83, and 0.66, respectively. Except for the sites where the peak yield for growing season is harvested, the modeled mean harvested yield is around 30 % lower than the simulated mean peak yield for each grass (Table 4). This is in agreement with recommended harvest management, which suggests that harvest until winter or early spring will induce approximately 33 % reduction from peak biomass [4]. However, there are still some specific sites where the model is unable to accurately capture the observed yields.

The PBIAS values for Miscanthus yield are −66.7 % for Booneville, AR, site, −35.7 % for Stillwater, OK, site, and 54.6 % for Kingsville, TX, site, respectively (Table 4), indicating the overestimation of Miscanthus yield at Booneville and Stillwater sites, but the underestimation at the Kingsville site. The sampling variability (Table 4) is equal to 58, 60, and 66 % of measured mean yields at Booneville, Stillwater, and Kingsville, respectively. The higher sampling variability at the three sites suggests that there is a large environmental heterogeneity at each site, and ISAM is unable to capture the heterogeneity effect on spatial yield.

For Cave-in-Rock (Table 4), ISAM underestimates yield at two TX sites: Weslaco (PBIAS=57.8 %) and Kingsville (PBIAS=34.2 %). The sampling variability is also high at these two sites, which is equal to around 50 % of measured mean yields. This indicates that ISAM fails to capture large environmental heterogeneity at these two sites. The higher model bias is also observed at the Brownstown, IL, site, where the modeled yield for Cave-in-Rock is about 31 % higher than observed yield (Table 4). According to Dohleman [53], this site has a poor soil quality and weed pressure that might have slowed down the establishment of Cave-in-Rock and thus produced relatively low yield. However, ISAM is not able to capture the poor soil quality effect due to uncertainty in soil data used in our calculation, nor ISAM accounts for weed pressure effects.

In the case of Alamo yield, the largest model bias is observed at Jackson, TN, site, where the model overestimates yield with the bias magnitude of 45.1 % (Table 4). The Jackson site has a shallow soil depth and thus low water capacity, which limits the root development and lowers the yield due to water stress conditions [54]. The model is unable to simulate shallow soil depth and its effects on soil water capacity due to lack of high-resolution bedrock data, leading to overestimation of Alamo yield at this site. Otherwise, higher PBIAS values (Table 4) at the Kingsville, TX (PBIAS=41.4 %) and the Weslaco, TX (PBIAS=32.2 %) sites indicate that the model also underestimates Alamo yields at two sites due to the same reason discussed above.

The comparisons between modeled and measured SD values for yields at different sites indicate that the model is able to capture the measured yearly yield variability at most of the sites (Table 4), with the following exceptions: at the Elsberry, MO, site, the measured yearly yield variability for Miscanthus (16.1 t/ha) is seven times higher than the modeled yield variability (2.2 t/ha). Kiniry et al. [32] indicates that the maximum Miscanthus LAI at this site increases from 3.6 in 2010 to 7.6 in 2011 and thus leads to almost two times of increase in yield from 2010 to 2011. However, the model is unable to capture this yearly increase in maximum LAI and thus the yield during the second and the third year after establishment. For Cave-in-Rock, the measured yield variability at the Kingsville, TX, site (1.6 t/ha) is seven times higher
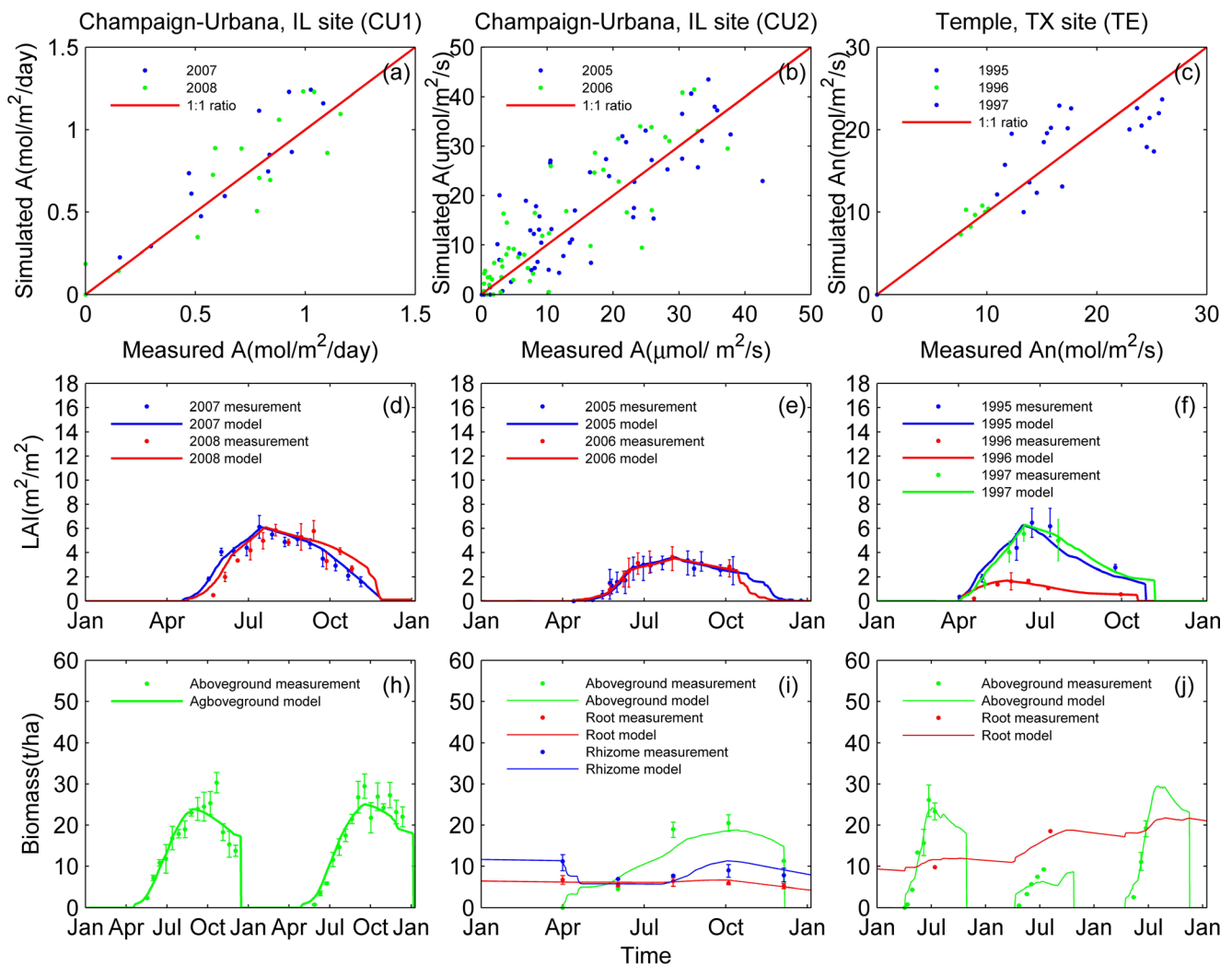
Fig. 2 Measured and model simulated carbon assimilation rates (A/An) (**a**–**c**), LAI (**d**–**f**), and biomass (aboveground, root and rhizome) (**h**–**j**) for Miscanthus at Urbana, IL, Cave-in-Rock at Urbana, IL, and Alamo at Temple, TX, sites. Here A is the daily gross carbon assimilation rate at leaf level for Miscanthus and the hourly gross carbon assimilation rate at canopy level for Cave-in-Rock. An is the net carbon assimilation rate for Alamo at leaf level. The data for Miscanthus is for the time period 2007–2008, for Cave-in-Rock 2005–2006, and for Alamo 1995–1997. The biomass data for Cave-in-Rock is only available as the multiyear mean values over the time period 2005–2006

than the modeled yield variability (0.2 t/ha). The mismatch between modeled and measured yearly yield variability at this site could be due to the same reasons as discussed above. The apparent underestimation of modeled yearly variability in Alamo yield is shown at the Nacogdoches site, the Blacksburg site, the Jackson site, and the Kingsville site (Table 4). The underestimation of yearly variability in Alamo yield at the Nacogdoches site is due to underestimation of yearly maximum LAI variability during the second and the third year after establishment, while the disagreement between modeled and measured yearly yield variation at the Jackson site and Kingsville site is due to lack of high-resolution bedrock data or lack of large spatial heterogeneity of environmental factors within the site as discussed above. The Blacksburg site is situated on a steep slope and thus has a low water infiltration [55], which

leads to a strong sensitivity of Alamo yield to precipitation. ISAM currently fails to capture steep slope conditions and hence the lower water infiltration. Most of the trial sites selected for our analysis have multiple years of data sets, with the exception of three Miscanthus sites in Florida. We include these three sites in our model analysis because there are not many sites available in the literature for Miscanthus yield data in Florida. The statistical analysis suggests that accounting of these three sits does not skew the statistics for evaluating the model performance on Miscanthus yield simulation. The re-calculate *dr* value without including these three sites was as high as 0.85, which was not significantly different than with including case value of 0.87.

In summary, the model is able to capture observed mean yields and their variations for three energy grasses under

Table 4 Mean and standard deviation (SD) from the mean for modeled and measured yields, modeled peak yield for growing season, sampling variability in measured yield, relative percent bias (PBIAS) in modeled yield for each validation site (Miscanthus: M1-M17; Cave-in-Rock: C1-C28; Alamo: A1-A22). Here N is the number of years for measured data and mean is calculated for N years

Site ID	Sites	State	Latitude (°)	Longitude (°)	N	Mean and SD(±) for measured yield (t/ha)	Mean and SD(±) for modeled yield (t/ha)	Modeled mean peak yield (t/ha)	Sampling variability (t/ha)	PBIAS (%)
M1	Mead	NE	41.17	−96.47	2	21.3±5.6	18.3±3.8	26.1	−	14.1
M2	Adelphia	NJ	40.23	−74.25	2	12.4±2.9	13.6±2.7	19.7	−	−9.7
M3	Champaign	IL	40.03	−88.23	2	17.9±4.1	19.8±2.2	31.5	−	−10.6
M4	Troy	KS	39.77	−95.2	2	8.9±4.9	7.0±2.6	9.7	−	20.9
M5	Manhattan	KS	39.18	−96.58	2	7.3±4.6	6.8±2.5	9.3	−	6.9
M6	Elsberry[a]	MO	39.16	−90.79	2	33.7±16.1	27.9±2.2	27.9	4.8	17.2
M7	Columbia[a]	MO	38.89	−92.19	2	21.6±5.8	24.1±3.7	24.1	7.6	−11.8
M8	Lexington	KY	38.13	−84.5	2	17.4±0.9	18.3±0.8	23.9	−	−5.5
M9	Mt. Vernon[a]	MO	37.07	−93.81	2	13.9±3.2	14.6±1.1	14.6	7.0	−5.0
M10	Stillwater	OK	36.12	−96.05	2	3.0±0.5	4.0±1.8	4.0	1.8	−35.6
M11	Fayetteville[a]	AR	36.09	−94.11	2	10.5±1.4	10.9±1.0	10.9	4.4	−3.8
M12	Booneville[a]	AR	35.08	−93.98	1	4.5	7.5	7.5	2.6	−66.7
M13	Nacogdoches[a]	TX	31.5	−94.6	2	4.0±1.2	4.3±2.2	4.3	3.0	−7.6
M14	Gainesville[b]	FL	29.65	−82.33	1	6.2	6.8	8.0	−	−9.7
M15	Kingsville[a]	TX	27.54	−97.85	2	5.4±0.3	2.5±0.7	2.5	3.6	54.6
M16	Ona[b]	FL	27.48	−81.92	1	4.5	4.7	7.7	−	−4.4
M17	Belle Glade[b]	FL	26.68	−80.67	1	10.8	11.0	13.6	−	−1.9
C1	Dickinson	ND	46.88	−102.8	3	4.5±0.9	4.3±0.9	6.4	−	5.1
C2	Mandan	ND	46.8	−100.92	3	5.5±2.7	5.9±2.0	7.8	−	−8.5
C3	Brookings	SD	44.02	−97.09	4	3.9±0.5	3.9±1.2	6.2	−	−1.9
C4	Arlington	WI	43.33	−89.38	4	14.3±3.2	12.1±1.1	14.2	−	15.4
C5	Dekalb	IL	41.85	−88.85	4	8.4±1.8	9.2±2.5	13.9	2.4	−9.6
C6	Champaign	IL	40.08	−88.23	2	12.7±2.1	12.3±2.2	17.3	4.3	3.2
C7	Orr	IL	39.81	−90.82	3	10.0±1.0	10.7±1.0	16.2	1.2	−7.0
C8	Morgantown	WV	39.62	−79.95	3	14.7±0.7	14.2±1.6	18.2	−	3.6
C9	Elsberry[a]	MO	39.16	−90.79	2	13.6±2.2	14.5±2.3	14.5	2.8	−6.2
C10	Brownstown	IL	38.95	−88.96	3	8.2±2.4	10.8±1.1	13.8	1.0	−30.8
C11	Columbia	MO	38.89	−92.19	2	8.2±0.8	9.5±0.7	11.3	2.6	−16.0
C12	Fairfield	IL	38.35	−88.35	3	14.7±0.9	14.0±1.3	18.1	2.1	4.5
C13	Dixon Spring	IL	37.45	−88.67	4	10.8±3.4	10.7±2.1	14.7	4.2	0.7
C14	Princeton	KY	37.1	−87.82	3	11.8±1.3	10.3±0.6	14.1	−	12.4
C15	Mr. Vernon[a]	MO	37.07	−93.81	2	9.9±4.9	12.4±3.4	12.4	3.0	−24.7
C16	Stillwater[a]	OK	36.12	−96.05	2	11.6±1.0	11.9±0.9	11.9	3.0	−2.6
C17	Fayetteville[a]	AR	36.09	−94.11	2	10.1±0.3	11.2±0.4	11.2	5.0	−11.4
C18	Knoxville	TN	35.88	−83.95	3	13.6±0.8	12.0±1.8	17.1	−	11.3
C19	Raleigh	NC	35.72	−78.67	3	8.2±1.8	8.7±0.5	12.3	−	−6.1
C20	Jackson	TN	35.62	−88.83	3	8.1±0.3	7.4±0.1	10.7	−	7.9
C21	Chickasha	OK	35.03	−97.91	7	7.6±1.8	6.6±1.8	9.7	−	13.9
C22	Dallas	TX	32.97	−97.27	4	5.0±2.9	4.2±0.9	5.7	−	15.2
C23	Nacogdoches[a]	TX	31.5	−94.6	2	4.7±1.6	5.4±2.2	5.4	2.6	−14.9
C24	Temple	TX	31.06	−97.22	4	3.9±2.1	4.2±0.9	5.7	−	−9.1
C25	College station	TX	30.6	−96.35	3	6.4±3.2	6.0±1.5	6.4	−	6.2
C26	Beeville	TX	28.4	−97.7	4	3.7±1.8	2.9±2.5	2.6	−	7.3
C27	Kingsville[a]	TX	27.54	−97.85	2	3.7±1.6	2.4±0.2	2.4	1.8	34.2
C28	Weslaco[a]	TX	26.22	−98.13	2	4.2±2.2	1.8±0.9	1.8	2.1	57.8
A1	Morgantown	MV	39.62	−79.95	6	16.4±1.1	15.1±1.1	20.2	−	7.9

Table 4 (continued)

Site ID	Sites	State	Latitude (°)	Longitude (°)	N	Mean and SD(±) for measured yield (t/ha)	Mean and SD(±) for modeled yield (t/ha)	Modeled mean peak yield (t/ha)	Sampling variability (t/ha)	PBIAS (%)
A2	Elsberry[a]	MO	39.16	−90.79	2	20.8±0.9	21.1±2.0	21.1	5.5	−1.4
A3	Columbia	MO	38.89	−92.19	2	16.4±4.6	19.2±4.6	19.2	6.1	−17.1
A4	Orange	VA	38.22	−78.12	6	17.2±1.8	17.4±1.1	22.8	−	−1.2
A5	Blacksburg	VA	37.18	−80.42	6	14.3±3.0	15.1±0.7	21.9	−	−5.4
A6	Princeton	KY	37.1	−87.82	6	14.1±1.6	14.8±0.7	22.7	−	−5.0
A7	Mt. Vernon[a]	MO	37.07	−93.81	2	16.2±1.1	16.7±1.1	16.7	5.6	−3.1
A8	Stillwater[a]	OK	36.12	−96.05	2	13.6±1.5	11.8±3.4	11.8	5.6	12.9
A9	Fayetteville[a]	AR	36.09	−94.11	2	14.9±1.1	16.5±1.0	16.5	4.9	−11.1
A10	Knoxville	TN	35.88	−83.95	6	21.7±2.2	19.7±2.2	19.7	−	9.3
A11	Raleigh	NC	35.72	−78.67	6	12.3±3.2	12.5±1.0	20.1	−	−1.8
A12	Jackson	TN	35.62	−88.63	6	9.8±2.0	14.2±0.5	22.1	−	−45.1
A13	Hope	AR	33.67	−93.58	1	16.8	15.4	23.8	−	8.3
A14	Dallas	TX	32.97	−97.27	4	8.1±5.3	9.2±3.9	14.5	−	−12.9
A15	Stephenville	TX	32.22	−98.2	1	10.9	10.0	15.4	−	8.3
A16	Nacogdoches[a]	TX	31.5	−94.6	2	22.9±10.4	19.5±2.4	19.5	9.9	15.1
A17	Temple	TX	31.06	−97.22	4	14.4±2.4	13.9±0.9	19.3	−	3.1
A18	Clinton	LA	30.85	−90.05	1	10.7	12.9	20.2	−	−21
A19	College station	TX	30.6	−96.35	4	15.4±3.2	14.3±2.9	20.8	−	7.2
A20	Beeville	TX	28.4	−97.7	3	12.7±3.9	11.0±3.6	17.6	−	13.4
A21	Kingsville[a]	TX	27.54	−97.85	2	22.9±3.9	13.4±1.0	13.4	9.4	41.4
A22	Weslaco[a]	TX	26.22	−98.13	2	22.8±3.3	15.5±6.6	15.5	15.1	32.2

[a] Yield is harvested at the time of peak biomass

[b] Based on first year of yield data

diverse environmental conditions in the USA. The high model biases for some sites in extreme southern TX are due to site-level environmental heterogeneity not captured in the model. The uncertainty in bedrock and slope data sets also explains the model biases in Alamo yields and their variations at specific sites.

Estimating Yield Zones Based on Spatial and Temporal Variations for Biomass Yield for Energy Grasses

Information on potential bioenergy yields in space and time will be crucial in order to improve estimation of feedstock supply areas for biorefineries and to reduce biomass producer risk [56]. However, spatial variations for bioenergy feedstock could vary with time and space due to changes in environmental conditions, such as temperature and precipitation, and soil characteristics. Here, we carried out quantitative analysis of biomass yield of bioenergy grasses to identify the spatial and temporal trends in the USA using the methodology described by Blackmore et al. [57] and later on applied by other studies [56]. This methodology identifies the regions where yields could be high or low and stable or unstable in time.

In order to estimate spatial and temporal pattern of biomass yields over the period 2001–2012, the model is first initialized

with NLDAS-2 climate [44] and STATSGO2 soil database [45] along with current land cover and atmospheric CO_2 concentrations for year 2000 until soil temperature and moisture reach steady state. Energy grasses were then planted with commonly reported seedling and rhizome planting densities, which were 4,850 rhizomes/acre (approximately 600 kg/ha) for Miscanthus [58] and 8.5 kg/ha of seeds for Cave-in-Rock and Alamo [59]. We follow the agronomic practices to grow switchgrass and Miscanthus at site level calculations based on the information provided in the literature for each site. For the US-scale calculations, we prescribe agronomic practices based on Lee et al. [60].

Here, we use spatial yield patterns estimated by ISAM at $0.5° \times 0.5°$ to assess the regions which continuously produce higher (or lower) yields due to favorable (or unfavorable) conditions, such as soil and topography characteristics and regional climate conditions. A single spatial yield pattern of each bioenergy grass is presented as the arithmetic mean (AM) of yearly yield for the period 2001–2012 at each grid point. Here, we exclude low and unstable yield in the establishment year at each grid point. The thresholds, which classify high and low yield zones, are defined as the median value of the AM of yield over the period 2001–2012 for all grid cells. To quantify the effects of environmental factors on spatial

yield pattern, the statistical significance of the differences in environmental variables between high and low yield zones is analyzed by rank-sum test [61] and comparing the median values of each environmental variable for high and low yield zones. The environmental variables considered here include the following: mean air temperature (T), mean short wave radiation (Ra), accumulated precipitation (P), and mean Wa during the growing season and photoperiod during the vegetative stage (L_{day}). The value of each environmental variable at each grid point is expressed as its multi-year mean values over the time period 2001–2012.

The yearly variations in yield over the period 2001–2012 at each model grid are used to assess the extent to which yields vary temporally. The degree of temporal variability in yields is measured as temporal variance defined as the square of the standard deviation (SD^2) at each grid cell [57]. The lower the variance is, the lower the extent to which yield varies temporally due to variation in weather conditions, and thus the greater the temporal yield stability. The threshold values of temporal variance in yield are used to define stable ($SD^2 \leq$ threshold) and unstable ($SD^2 >$ threshold) yields for each bioenergy grass. The threshold value for temporal variance in yield can be assigned according to multiple criteria and could include choosing a fraction of the coefficient of variation or relating it to potential management practices [57]. We assign the threshold value of temporal variance for each bioenergy crop where SD (the square root of the temporal variance) is about 16 % of the bioenergy's median crop yield (values defined above). A sensitivity analysis suggests that choosing a threshold value based on SD being greater than about 16 % results in an insignificant number of grid points being identified as unstable.

To quantify how variability in climate variables influences temporal yield variability, we calculate the coefficient of variation (CV) for each climate variable over the time period 2001–2012 at each grid cell. CV defines as the percentage fraction of standard deviation of each climate variable to its mean value over the time period 2001–2012, and thus indicates the relative variability of each climate variable relative to its mean value. The significance of difference in CV values of each climate variable between stable/ unstable yields zone is firstly tested through rank-sum test and then quantified by comparing estimated median values for CV in stable/unstable yield zones. Since soil texture can influence the sensitivity of yield to variability in climate variables, here we also calculate the CV values for Wa over the same period and compare its difference between stable/unstable yield zones.

After assigning the threshold values for high/low yield classification and stable/unstable yield classification, the spatial trend and temporal variations are then grouped together into four yield class zones: high and stable yield zone (HS), high and unstable yield zone (HU), low and stable yield zone (LS), and low and unstable yield zone (LU). The HS yield zone is more appropriate to grow bioenergy grasses with stable high yields, whereas the yield in HU zone is sensitive

to the variance in weather variables. The LS yield zone is not appropriate to grow bioenergy grasses due to unfavorable climate and soil characteristics. Finally, yields in LU zones are uncertain due to high variance. Future climate change that may increase precipitation may increase the yield in this zone.

Estimated Spatial Yield Patterns for Energy Grasses

The model simulates no establishment of Miscanthus in the region above the PHZ 4 (Fig. 3a). This is in agreement with most field experiments, which fail to establish Miscanthus in upper Michigan, the northern part of lower Michigan, as well as northern Vermont, New Hampshire, and Maine. The extreme low over-winter temperatures in these regions induce almost 100 % rhizome mortality and thus no survival of Miscanthus. In addition, the model also simulates no survival of Miscanthus in the western Great Plains (Fig. 3a) where accumulated precipitation over the growing season is estimated to be less than 400 mm (Figure S2a). Except for region with no survival of Miscanthus, there are large spatial variations with average annual yields for the time period 2001–2012 ranging between 2 and 25 t/ha. High-yield zones with yield of more than 15 t/ha are located in the central Midwest, Kentucky, Tennessee, and the upper south Atlantic region. The results suggest that there are significant differences in P, mean Wa, mean Ra, and mean T_g during the growing season and mean photoperiod during the vegetative stage (Table 5) between high/low yield zone for Miscanthus. In addition, the results indicate that high yields are supported by high precipitation ($P > 600$ mm), moist soil condition, T_g less than 296 K, and longer mean photoperiod during the vegetative stage (Figure S2a, g, j). In contrast, low precipitation amount reduces Wa for the Miscanthus growth in the eastern Great Plains, leading to less than 10 t/ha of yield (Fig. 3a), whereas the low Miscanthus yields in the southern USA are due to too warm conditions ($T_g > 296$ K). High temperature reduces carbon assimilation rates and thus the yield in this region. Moreover, too warm condition here delays the senescence process and reduces N translocation, leading to N limitation for the growth in the following year. In addition, shorter than normal day length in the southern USA induces earlier flowering time, which reduces leaf size and number and thus carbon assimilation [34].

Similar to Miscanthus, the model simulates no survival of Cave-in-Rock in the western part of Great Plains, mainly the region located in the west of the 100th meridian. Limited precipitation together with poor soil texture in the northwest of Nebraska induces strong water limitation on the establishment of Cave-in-Rock. Cave-in-Rock could survive in most of the rest part of the eastern USA, except for region above PHZ 3, where grass may not survive due to too cold winter conditions. The Cave-in-Rock yield in its establishment region has an estimated range between 2 and 15 t/ha, with the critical value for classifying high/low yield zone of 9.4 t/ha. Cave-in-
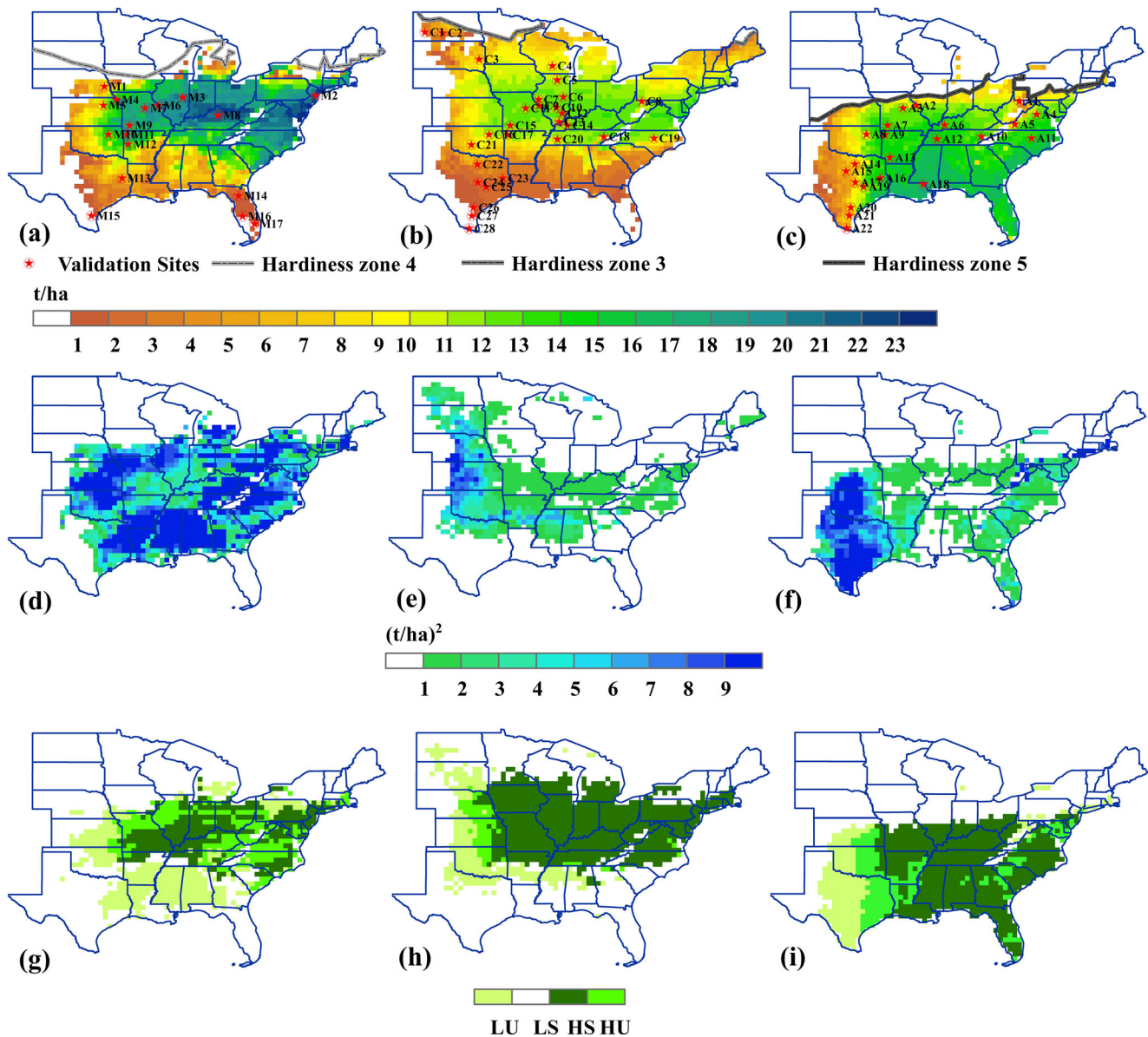
Fig. 3 The spatial yield patterns (Miscanthus (**a**), Cave-in-Rock (**b**), and Alamo (**c**)), the temporal yield variance maps (Miscanthus (**d**), Cave-in-Rock (**e**), and Alamo (**f**)), and the spatial and temporal yield trend maps (Miscanthus (**g**), Cave-in-Rock (**h**), and Alamo (**i**)) for three energy crops. In the legend of figures **g**, **h** and **i** the *HS* represents high and stable yield zone, *HU* high and unstable yield zone, *LS* low and stable yield zone, and *LU* low and unstable yield zone

Rock can share the same high yield zone as that for Miscanthus (Fig. 3b). In addition, there is also high yield in Iowa, eastern Nebraska, eastern Kansas, and eastern Oklahoma. Table 5 suggests that the high Cave-in-Rock yield zones are attributed to high precipitation ($P > 500$ mm), moist soil condition, and suitable temperature ($T_g > 296$ K) during the growing season and longer mean photoperiod during the vegetative stage (Figure S2b, h, k). Yields in central Great Plains (Fig. 3b) are low due to less than 500 mm of precipitation during the growing season together with poor soil texture, which limits the water availability for Cave-in-Rock growth (Figure S2b, k). As discussed for Miscanthus, lower Cave-in-Rock yields (<6 t/ha) in the southern USA are due to too hot conditions and shorter than normal day length.

Unlike Miscanthus and Cave-in-Rock, Alamo may not be established in most of the northern USA. This is agreement with the field experiments, which suggest that Alamo usually could not adapt to the region above PHZ 6 because unfavorable cold winter conditions, which could induce almost 100 % of rhizome mortality [7]. In addition, Alamo may not survive in the western Texas due to too dry condition in this region. Alamo yields in the rest of the eastern USA have the range between 4 and 17 t/ha, with the critical value for classifying high/low yield zone of 11 t/ha. The most parts in the bottom of

Table 5 Annual median values for various environmental factors averaged over the period 2001–2012. The values are provided for high and low yield zones for three energy crops

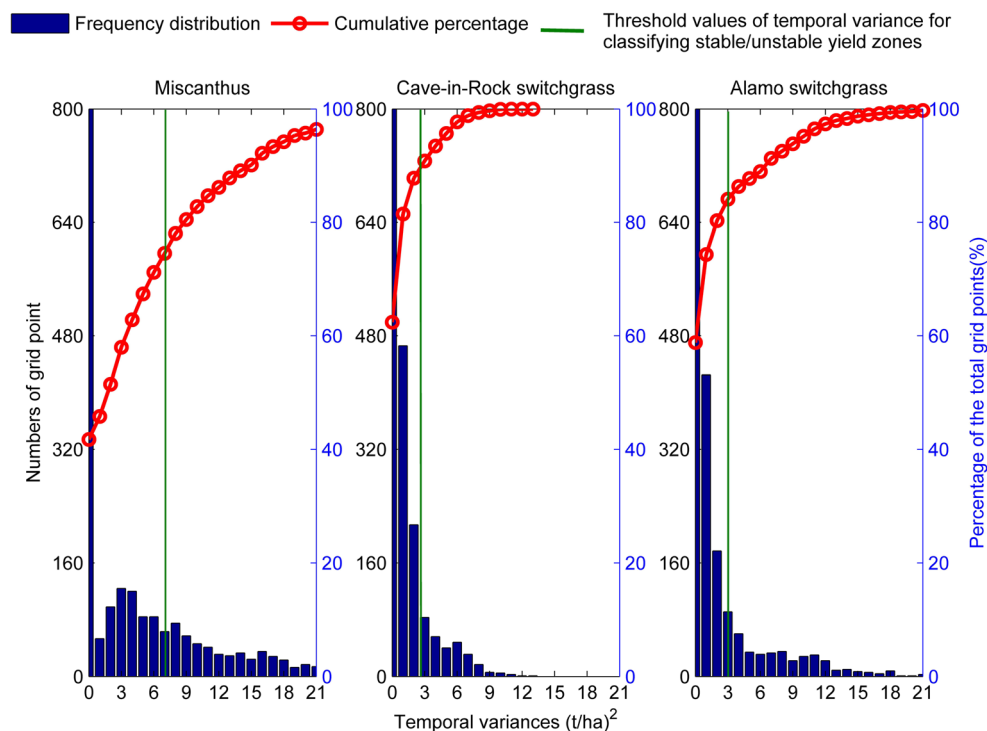| Bioenergy grass	Yield zone	Environmental factors				
		Accumulated precipitation (P) [mm]	Radiation (Ra) [MJ]	Temperature (T_g) [MJ]	Soil water availability index (Wa)	Photoperiod (L_{day}) [h]
Miscanthus	High	749[a]	19[a]	293[a]	1.00[a]	14.6[a]
	Low	704[a]	22[a]	297[a]	0.96[a]	14.0[a]
Cave-in-Rock	High	669[a]	20[a]	293[a]	1.00[a]	14.6[a]
	Low	603[a]	18[a]	297[a]	0.95[a]	14.1[a]
Alamo	High	754[a]	21	296	1.00[a]	14.0[a]
	Low	610[a]	20	296	0.93[a]	14.6[a]

[a] Variable value is statistically significantly different from Low/High yield zone. The statistical test is performed with rank-sum test. The significance level for statistical analysis, α, is 0.01

the Midwest, Atlantic Plains, and most of the southern USA are identified as high yield zones, except for central Kansas, central Oklahoma, and central Texas. Table 5 shows that P and mean Wa during the growing season are significantly higher in the high Alamo yield zone than that in the low yield zone, whereas photoperiod during the vegetative stage is significantly lower in the high yield zone than that in the low yield zone. This analysis suggests that high precipitation ($P > 600$ mm), moist soil condition during the growing season (Figure S2 c, l), and relatively short photoperiod results in the high Cave-in-Rock yield. Low yields in central Kansas, central Oklahoma, and central Texas are attributed by low precipitation and thus low Wa in the region.

Temporal Yield Variations for Energy Grasses

The estimated SD^2 range between 0 and $64\,(t/ha)^2$ for Miscanthus, $0–13\,(t/ha)^2$ for Cave-in-Rock, and $0–24\,(t/ha)^2$ for Alamo over the USA (Fig. 3d–f). Given the median yield values for three bioenergy crops, the threshold values for classifying stable/unstable yield zones are therefore $7.0\,(t/ha)^2$ for Miscanthus, $2.5\,(t/ha)^2$ for Cave-in-Rock, and $3.0\,(t/ha)^2$ for Alamo. Figure 4 shows the distribution of SD^2 across all grid points, as well as the thresholds for temporally stable yields. This curve indicates that the percentage of the total number of grid cells with temporally stable yield apparently increases with increasing level of temporal variance, but

Fig. 4 The *bar chart* shows the distribution of total number of grid points falling into the each bin of variance interval and the *curve* shows the variation of the percentage of total number of grid points, with increasing values of the temporal yield variance for Miscanthus, Cave-in-Rock, and Alamo yields over the US domain. The *green vertical line* shows the threshold value for temporal variance for classifying stable/unstable yield zones

with gradually decreasing rates, as indicated by the first deviation of the curve in Fig. 4. The total grid cells that have temporal yield variances lower than or equal to these thresholds are 75 % of Miscanthus, 89 % of Cave-in-Rock, and 84 % of Alamo. However, only 21 % of these stable yield zones for Miscanthus, 41 % of stable yields zones for Cave-in-Rock, and 16 % of stable yields zones for Alamo can be considered as high yield zones.

Except for the region in bottom of the Midwest, western Kentucky, western Tennessee, as well as central Texas, southern Oklahoma, and eastern Nebraska, Miscanthus yields in the rest of the eastern USA are unstable (Fig. 3d). Table 6 shows that the CV values for both precipitation and Wa in the unstable yield zones are significantly higher than that in the stable yield zone. These results explain unstable Miscanthus yields in eastern Kansas and northern Oklahoma, where more than 20 % of relative variability in precipitation together with poor soil texture induces more than 10 % of relative variability of Wa (Figure S3a, d) and thus drives high yield variations for Miscanthus. Relative to these regions, similar variability in precipitation does not induce high variability in soil water availability in moist southern USA (Figure S3a, d). Table 6 indicates significant difference in radiation and temperature between stable/unstable Miscanthus yield zones. Our study indicates that more than 4 % of relative variability in radiation following variability in precipitation amount (Figure S3g) drives unstable Miscanthus yields in the southern USA (Fig. 3d). The higher radiation and temperature variability (>6 %) in the unstable yield zones mainly control the higher yield variability in the central Midwest, such as northern Missouri, northern Illinois, southern Michigan, Ohio, and the western Pennsylvania in the northeastern USA (Fig. 3d).

Unlike Miscanthus, Cave-in-Rock yield is stable in most of the eastern USA, except the regions discussed as follows. Table 6 suggests that high variability of precipitation, Wa, radiation, and temperature induce unstable Cave-in-Rock yield. The unstable yields in the eastern Great Plains (Fig. 3e) are due to more than 20 % of precipitation relative variability and thus high variability in Wa (Figure S3b, e). In addition, high relative variability in temperature (CV>7 %) (Figure S3k) also attributes to the unstable Cave-in-Rock yield in South Dakota and North Dakota (Fig. 3e). Cave-in-rock yields in southern Arkansas and northern Mississippi are very sensitive to radiation variation (Figure S3h), even 3 % of relative variability in radiation could induce more than $5(t/ha)^2$ of yield variation in this region.

For Alamo, the unstable yield zones are mainly located in eastern Kansas, eastern Oklahoma, eastern Texas, and the connection region between Arkansas and Louisiana (Fig. 3f). The significant difference in precipitation and Wa between stable/unstable yield zones (Table 6) indicates that high Alamo yield variability here is the response to high precipitation and Wa variability (Figure S3c, f). In addition, there is also unstable Alamo yield in West Virginia and Maryland (Fig. 3f), which is related to high relative variability of temperature in this region (Figure S3l).

Homogeneous Spatial Zones Based on the Spatial and Temporal Trends in Yield for Energy Grasses

Figure 3g–i shows that all three zones (HU, LU, LS) are usually successively distributed, northward, southward, and westward from HS zones for Miscanthus and Cave-in-Rock, but northward and westward from HS zones for Alamo.

There are some common trends for three bioenergy grasses in the distribution of yield zones in the USA. The HS yield zones for three bioenergy grasses are in southern Missouri, northwestern Arkansas, southern Illinois, southern Indiana, southern Ohio, western Kentucky, and part area of northern Virginia (Fig. 3g–i). The highest Miscanthus yield is almost 1.8 and 1.5 times higher than that for Cave-in-Rock and Alamo in these regions. The LS yield zones for Miscanthus and two cultivars of switchgrasses are located in the upper part of north central, northeastern, and northern New England as well as western parts of Great Plains (Fig. 3g–i). Three bioenergy grasses usually could not be established in these regions (Fig. 3a–c).

Parts of the Midwest region, such as northern Illinois, Indiana and Ohio, and eastern Kentucky are HU yield zones

Table 6 Annual median values of coefficient of variance (CV) averaged over the period 2001–2012 for various input variables. The values are provided for stable and unstable yield zones for three energy crops

Bioenergy grass	Yield zone	CV of accumulated precipitation [%]	CV of radiation [%]	CV of temperature [%]	CV of water availability [%]
Miscanthus	Stable	20.5[a]	3.8[a]	4.1[a]	4.2[a]
	Unstable	25.0[a]	4.3[a]	4.7[a]	5.1[a]
Cave-in-Rock	Stable	22.9[a]	3.3[a]	4.7[a]	1.7[a]
	Unstable	27.0[a]	4.4[a]	5.0[a]	11.8[a]
Alamo	Stable	24.0[a]	4.1	3.9[a]	1.3[a]
	Unstable	29.4[a]	4.0	4.4[a]	18.2[a]

[a] Variable value is statistically significantly different from Low/High yield zone. The statistical test is performed with rank-sum test. The significance level for statistical analysis, α, is 0.01

for Miscanthus (Fig. 3g) and HS zones for Cave-in-Rock (Fig. 3h), but LS yield zones for Alamo (Fig. 3i). Most of the areas in Tennessee, southern Virginia, and North Carolina are HS yield zones for Cave-in-Rock and Alamo, but HU yield zone for Miscanthus. Most areas of the southern USA are the HS yield zone for Alamo, but the LU yield zone for Miscanthus and LS yield zone for Cave-in-Rock. In eastern parts of Great Plains, both Cave-in-Rock and Alamo show the transition from HU to LU yield zones along an east-to-west gradient. However, Miscanthus is usually low and unstable in this region.

Overall, the HS yield zones for the three bioenergy grasses discussed here are more suitable to grow bioenergy grasses with minimum natural resource investment. Extra management practices such as irrigation, especially in the dry year, might help to increase the stability of bioenergy grass yields in the HU yield zones. Upper part of north central, northeastern, and northern New England and western parts of Great Plain, defined as LS yield zones, are not appropriate to grow Miscanthus and Cave-in-Rock and Alamo switchgrasses. There could be some other bioenergy crops or other switchgrasses cultivars that may be grown in this region.

Comparing ISAM Estimated Bioenergy Yields with Other Studies

We compare ISAM estimated biomass yields for energy crops with previously published model studies that simulate bioenergy yields either at a regional or US scale, including Miguez et al. [17, WIMOVAC (BIOCRO) model], VanLoocke et al. [18, Agro-IBIS model], Zhuang et al. [20, TEM model], Jager et al. [9, empirical model], Thomson et al. [16, EPIC model], and Behrman et al. [12, ALMANAC model]. The major characteristics and the main results of these models along with ISAM are listed in Table 7. All models, with the exception of Jager et al. [9], are process-based models, which simulate carbon assimilation and allocation processes for Miscanthus and/or switchgrasses. Among these models, the EPIC and ALMANAC models use radiation use efficiency to calculate switchgrass yields [12, 16], while other models use more detailed biophysical methods to simulate carbon assimilation. The major distinction between ISAM and other models is that ISAM is the only model which accounts for dynamic response of carbon allocation, LAI growth, as well as root growth and distribution among the soil layers to environmental factors, such as precipitation, temperature, and radiation. Similar to EPIC and ALMANAC model, ISAM also parameterizes Cave-in-Rock and Alamo separately.

In terms of Miscanthus yield, ISAM estimates consistently higher yields in the central and southern Midwest Corn belt, which is similar to BIOCRO, Agro-IBIS, and TEM models. However, the ISAM estimated highest yield in this region, which is 25 t/ha and similar to TEM estimated highest yield

value of 21.5 t/ha, is almost 38 % lower than the BIOCRO model estimated highest yield of 40.5 t/ha and 31 % lower than the Agro-IBIS estimated highest harvested yield of 36 t/ha. This difference could be due to the fact that these two models use different sets of observation data to calibrate the model parameters. ISAM is calibrated based on the observation data from a large plot at Champaign-Urbana (plot size 0.2 ha) site, whereas BIOCRO and Agro-IBIS are calibrated based on observed data from a small plot at the same site (plot size 0.01 ha). Due to edge effects, the observed aboveground biomasses for the small plot for years 2007 and 2008 are as high as 2.9 times as compared to the observed data for the large plot [53, 62]. In addition, ISAM and BIOCRO model estimated spatial yield patterns differ in the south USA. ISAM estimated Miscanthus yield in the southern states, including eastern Texas, Louisiana, Mississippi, Alabama, Georgia, and Florida, is lower than 8 t/ha, but BIOCRO model estimated yield is usually higher than 20 t/ha in this region. Observed data (Table 4) from sites in Arkansas, Texas, Oklahoma, and Florida suggests that ISAM estimated Miscanthus yield in the southern USA is consistent with measured values at these sites, whereas BIOCRO model may have overestimated Miscanthus yield in the southern US.

For Cave-in-Rock switchgrass, all models, including ISAM, estimate higher yield for Illinois, Indiana, Ohio, Iowa, and Missouri. ISAM estimated highest yield for Cave-in-Rock in these states is 15 t/ha, which is consistent with ALMANAC estimated yield of 14 t/ha, but slightly higher than EPIC estimated highest yield of around 12 t/ha and TEM estimated highest yield of 10.8 t/ha (Table 7).

For Alamo switchgrass, all models simulate higher yield in the southern US states, including Louisiana, Mississippi, and Alabama. ISAM estimated highest yield for Alamo in these states is 17 t/ha. This estimated yield is consistent with EPIC estimated highest yield of 16 t/ha in this region and falls in the range (15–20 t/ha) of BIOCRO model estimated yields in this region. However, ISAM estimated yield along the Gulf coast and Florida (15–17 t/ha) is lower than ALMANAC estimated higher yield (>18 t/ha) for the same region. One of the reasons for this difference could be due to the fact that the two models follow different N management practices. The simulation with ALMANC applies 100 kg/ha N per year after establishment, whereas ISAM assumes no N fertilizer applications. This may have led to N limitation on Alamo growth in the ISAM simulated yield.

Overall, ISAM is able to simulate yields for bioenergy grasses under diverse environments conditions in the USA, especially in central and south of study domain, where model performances have been widely validated by the observed data. In north central, northeastern, and northern New England, an empirical function has been introduced to simulate the rhizome and stand mortality due to over-winter injury. Our model estimates less than 8 t/ha of Miscanthus yields in the most south part of Michigan, which is consistent with reported

Table 7 Comparison of simulated yields among different models

Model	Model characteristics	Maximum yield
ISAM (this study)	(1) Process-based biogeochemical model (2) Hourly time step over 1980–2010 period (3) 25×25 km spatial resolution (4) Biophysical approach for carbon assimilation (5) Dynamic carbon allocation factors, which account for interaction with environmental factors (6) Climate forcing: NLDAS data	Miscanthus: 25 t/ha in the USA Cave-in-Rock: 14 t/ha in the USA Alamo: 17 t/ha in the USA
BIOCRO model [17]	(1) Process-based model (2) Hourly time step over 1979–2010 period (3) 32×32 km spatial resolution (4) Biophysical approach for carbon assimilation (5) Dynamic carbon allocation factors which interact only with water availability (6) Climate forcing: temperature, precipitation, relative humidity, and wind speed from NCEP dataset, radiation data from NLDAS dataset	40.5 t/ha in the USA Switchgrass[a]: 20 t/ha in the USA
Agro-IBIS model [18]	(1) Process-based model (2) Hourly time step over 1973–2002 period (3) 0.5×0.5° spatial resolution (4) Biophysical approach for carbon assimilation (5) Fixed carbon allocation factors at each phenology stage (6) Climate forcing data: combination of University of East Anglia Climate Research Unit climatological datasets and NCEP daily anomaly dataset	Miscanthus: 36 t/ha in the Midwest USA Cave-in-Rock: 16 t/ha in the Midwest USA
TEM model [20]	(1) Process-based biogeochemical model (2) Monthly time step over 1990–1999 period (3) 25×25 km spatial resolution (4) Biophysical approach for carbon assimilation (5) Fixed carbon allocation factors (6) Climate forcing data: CRU dataset	Miscanthus: 21.5 t/ha grown on cropland in the USA Cave-in-Rock: 10.8 t/ha grown on cropland of the USA
Empirical model [9]	(1) Empirical model regressed with environmental variables (2) PRISM dataset	Upland switchgrass: 28 t/ha in the USA Lowland switchgrass: 40 t/ha in the USA
EPIC model [16]	(1) Processed-based model (2) Daily time step over 30 years (3) Radiation use efficiency method (4) Dynamic carbon allocation factors, which account for interaction with environmental factors	Switchgrass[a]: 16 t/ha in the USA
ALMANAC model [12]	(1) Process-based model with experimental simulation of LAI growth and biomass partitioning (2) Daily time step over 13 years (3) Radiation use efficiency (4) Calculate competition for water and nutrients among plants, biomass production, and biomass partitioning (5) Separate parameterization for upland and lowland switchgrasses (6) Application of 100 kg/ha nitrogen every year	Switchgrass[a]: 24.9 t/ha in the USA

[a] The study does not make distinction between various cultivars of switchgrass. The maximum yield here represents the maximum value among all switchgrass cultivars

Miscanthus yield range (1.47 to 9.0 t/ha) in this state [63]. This result suggests that the model is able to capture the effect of rhizome mortality due to over-winter injury. However, model estimated yield for Cave-in-Rock in this region is slightly higher (6.0–10.0 t/ha) as compared to measurements [63] (2.9 to 7.3 t/ha). We suggest that more observed data is needed in north central, northeastern, and northern New England to further validate our model performance. In addition, as discussed in model validation section, the model underestimates yields of bioenergy grasses at the bottom of southern Texas due to lack

of large spatial heterogeneity of environmental factors within specific sites. Thus, the potential yields of bioenergy grasses need to be further evaluated with high-resolution data for environmental variables, such as soil slope, soil depth, etc.

Conclusions

The study implements dynamic growth processes, including dynamic carbon allocation and root distribution, into a land

surface model, ISAM, with specific phenology development schemes for Miscanthus and Cave-in-Rock and Alamo. The simulated carbon assimilation rates, LAI, and carbon allocation among aboveground and belowground biomass for the three bioenergy grasses are in good agreement with observed data from Urbana, IL, site for Miscanthus and Cave-in-Rock, and a Temple, TX, site for Alamo. The modeled mean yield and its variation over measured years at 43 different evaluation sites are in good agreement with measured yields. The model calibration and evaluation results indicate that ISAM is able to capture the spatial and temporal variations in biomass yields for bioenergy grasses in the US.

Based on simulated mean bioenergy grass yields and their variances over the period 2001–2012 in the USA, we identify four yield zones: a high and stable yield zone (HS), a high but unstable yield zone (HU), a low and stable yield zone (LS), and a low and unstable yield zone (LU). Our results indicate that regional precipitation, temperature, soil water availability, and day length control the spatial distribution of high and low yields zones in the USA, whereas relative temporal variability in precipitation, temperature, and radiation determines the temporal stability and instability in the USA. The HS zone for the three bioenergy grasses is mainly located in the regions with precipitation greater than 600 mm and mean temperature 292–294 K during the growing season, and includes southern Missouri, northwestern Arkansas, southern Illinois, southern Indiana, southern Ohio, western Kentucky, and parts of northern Virginia. The highest yield for Miscanthus in these regions is 25 t/ha, which is about 1.8 and 1.5 times higher than the highest yield for Cave-in-Rock and Alamo in these regions. Besides the HS zones discussed above, Cave-in-Rock yields are also high and stable in northern Illinois, northern Indiana, and northern Ohio. Alamo yields are also high and stable in most areas of the southern USA, except for eastern Texas, the region between Arkansas and Louisiana, and the connect region among Tennessee, Georgia, and South Carolina. However, the lower part of the southern USA is usually a LU yield zone for Miscanthus and LS yield zone for Cave-in-Rock.

There are certain yield patterns, which are common to all three bioenergy grasses. These include the following: low and stable yield for all three grasses in the western Great Plains, such as western part of South Dakota, western Nebraska, western Kansas, western Texas, etc., due to poor soil texture and low precipitation; low and stable biomass yields in upper part of north central, northeastern, and northern New England due to cold temperature conditions. These LS yields zones are not suitable to grow three specific bioenergy grasses considered in this study, but it is likely possibly that other bioenergy crops or other switchgrasses cultivars perform better in these zones. However, the calculations of other bioenergy crops or switchgrasses cultivars are beyond the scope of this study and will be implement in the future modeling studies.

Overall, the ISAM-estimated spatial yields patterns for bioenergy grasses in the USA are in agreement with previous model studies. In addition, ISAM can simulate the adaption of different bioenergy grasses across the latitudes ranging between 26°N and 41°N for Miscanthus and between 26°N and 46°N for switchgrasses by accounting the effect of photoperiod on phenology and leaf development and the effect of extreme environmental conditions on establishment, carbon assimilation, and phenology. There are significant differences between the ISAM and other models estimated highest yields due to differences in the treatment of environmental stress factors in different models. With more comprehensive treatment of environmental factors, such as water, temperature, light, and nitrogen, on plant phenology and carbon allocation, ISAM estimated highest yield for bioenergy grasses is lower than BIOCRO and Agro-IBIS estimated values. For Miscanthus, these differences are also due to different observational data that is used for model calibration. ISAM is calibrated by data from a large plot at the Urbana-Champaign, IL, site, while BIOCRO and Agro-IBIS model are calibrated by data from a small plot. The observed aboveground biomasses from smaller plots were much higher than that from the larger plots due to the edge effects, and this effect should be accounted for if small plots are used for model calibration. The close agreement between the ISAM modeled and measured yields at extended evaluation sites (ranging from 26.68°N to 46.88°N) suggests that ISAM is able to simulate bioenergy grasses across diverse environments in the USA. Further evaluation of modeled yields in southern Texas is needed with high-resolution of soil depth and slope data. More measured yields data in north central, northeastern, and northern New England is also needed to further assess the model's performance in these areas.

The identification of four yield zones for bioenergy grasses in the eastern USA indicates that HS yield zones over most of eastern USA are more suitable to grow bioenergy grasses, whereas yield instability needs to be considered when assessing the potential yields of bioenergy grass in the HU yield zones. The LS yield zones in the upper part of north central, northeastern, and northern New England usually could not grow bioenergy grasses due to winter-injury. Bioenergy grasses also may not survive in western parts of Great Plains. Climate change may increase the uncertainty in yield variance in the HU and LU zones by altering the precipitation amount and frequency.

Appendix

Table 8 The values for various parameters used in this study. The three values separated by comma (,) the 'Values' column are for Miscanthus, Cave-in-Rock, and Alamo

Symbol	Definition	Values[a]	Source
P_{crit}	Critical precipitation over previous week for switchgrass seed planting	–, 6, 10 [mm]	This study
TP_{soil_crit}	Critical soil temperature for switchgrass seed planting	–, 288, 288 [K]	[8]
HUI0	Heat unit index above 0 °C	Vary	
GDD0	Accumulated growing degree days above 0 °C summed from the first day of the year to current running day during the simulation	Vary	
$GDD0_{max}$	Annual summation of growing degree days above 0 °C averaged for the 33 years (1980–2012)	Vary	Input parameters
$HUI0_e$	Minimum heat unit index above 0 °C during the emergence stage of phenology	0.10, 0.10, 0.10	Calibration parameter
$HUI0_{v1}$	Minimum heat unit index above 0 °C during the initial vegetative stage of phenology	0.12, 0.14, 0.14	Calibration parameter
$HUI0_{v2}$	Minimum heat unit index above 0 °C during the normal vegetative stage of phenology	0.30, 0.35, 0.22	Calibration parameter
$HUI0_{s1}$	Minimum heat unit index above 0 °C during the initial reproductive stage of phenology	0.66, 0.66, 0.41	Calibration parameter
$HUI0_{s2}$	Minimum heat unit index above 0 °C during the post reproductive stage of phenology	0.78, 0.73, 0.73	Calibration parameter
$HUI0_d$	Minimum heat unit index above 0 °C during the winter dormancy stage of phenology	1.0, 1.0, 1.0	Calibration parameter
D_e	Total maximum days during the emergence stage of phenology	8, 10, 10	Calibration parameter
D_{v1}	Total maximum days during the initial vegetative stage of phenology	50, 50, 50	Calibration parameter
D_{v2}	Total maximum days during the normal vegetative stage of phenology	60, 50, 60	Calibration parameter
D_{s1}	Total maximum days during the initial reproductive stage of phenology	60, 50, 50	Calibration parameter
D_{s2}	Total maximum days during the post reproductive stage of phenology	76, 56, 76	Calibration parameter
T_{base}	Base atmospheric temperature for grass planting and growth	283, 283, 285 [K]	[8, 40, 64]
T_{soil_crit}	Critical soil temperature for rhizome emergence	283, 283, 285 [K]	[4]
L_{day}	Day length in each day	Vary	
L_e	Critical day length for emergence	12,12,11	[8]
L_f	Critical day length for initiation of flowering	13, 13, 12 [h]	[33, 34]
LAI_{max}	Maximum leaf area index	6.0, 4.5, 6.0 [m^2/m^2]	[3, 46, 49]
LAI	Leaf area index	Vary	
T_{frost}	Air temperature critical value for frost damage	244, 239, 250 [K]	[7, 65]
T_{max_crit}	Temperature critical value for occurrence of extreme hot and dry	303, 300, 305 [K]	[37, 66]
T_{ymax}	Annual maximum air temperature averaged for the past 33 years (1980–2012)	Vary	Input parameter
T_{soil_s2}	Critical temperature for root zone	269, 269, 269 [K]	[8, 40]
T_{ytmin}	Annual minimum air temperature averaged for the past 33 years (1980–2012)	Vary	Input parameter
Wa_{crit}	The water availability critical value for extreme drought	0.50, 0.30, 0.65	Calibration parameter
T_{min3}	The previous 3 days average daily minimum temperature	Vary	

Table 8 (continued)

Symbol	Definition	Values[a]	Source
T_{min7}	The daily minimum temperature averaged for previous 7 days	Vary	
T_{max3}	The daily maximum temperature averaged for previous 3 days	Vary	
T_6	Previous 6 days average daily temperature	Vary	
P_7	The accumulated precipitation of previous week	Vary	
Wa_7	The mean water availability of previous week	Vary	
T_{avg_min}	Average annual extreme minimum temperature	Vary	Input parameter
ψ_b	The minimum water potential for switchgrass seed germination in Eq. A4	−0.3 [MPa]	[35]
T_{opt_g}	The optimal temperature for switchgrass seed germination in Eq. A5	–, 298, 303 [K]	[35]
T_{max_g}	The maximum temperature for switchgrass seed germination in Eq. A5	–, 315, 318 [K]	[35]
T_{base_g}	The base temperature for switchgrass seed germination in Eq. A5	–, 288, 288 [K]	[8]
θ_H	Hydro-condition variable for switchgrass seed germination in Eq. A3	Vary	
θ_T	Thermal condition variable for switchgrass seed germination in Eq. A3	Vary	
ψ	Mean water potential above top 3 cm of soil in Eq. A4	Vary	
ω	Sensitivity parameter of allocation to changes in availability of light, water and N	0.95, 0.8, 0.9	Calibration parameter
θ_t	Soil water potential at time step t	Vary	
θ_c	Soil water potential at the time of fully closing stomata	−275,000, −275,000, −275,000 [mm]	[27]
θ_o	Soil water potential at the time of fully opening stomata	−74,000, −74,000, −74,000 [mm]	[27]
φ	Soil porosity of the soil	Vary	
f_c	The ice fraction of soil	Vary	
Al_{e1}	Allocation fraction for leaf carbon during seed germination of switchgrass in the planting year in Eq. A6	–, 0.30,0.30	Calibration parameter
Ar_{e1}	Allocation fraction for root carbon during seed germination of switchgrass in the planting year in Eq. A6	–, 0.70, 0.70	Calibration parameter
Ah_e	Allocation fraction for rhizome carbon during emergence stage in Eq. A7	−0.02, −0.02, −0.01	Calibration parameter
Al_{e2}	Allocation fraction for leaf carbon during the emergence stage in Eq. A7	0.45, 0.60, 0.60	Calibration parameter
As_{e2}	Allocation fraction for stem carbon during the emergence stage in Eq. A7	0.25, 0.30, 0.30	Calibration parameter
Ar_{e2}	Allocation fraction for root carbon during the emergence stage in Eq. A7	0.30, 0.10, 0.10	Calibration parameter
Al_{v1}	Initial allocation fraction for leaf carbon during the initial vegetative stage	0.44, 0.50, 0.50	Calibration parameter
As_{v1}	Initial allocation fraction for stem carbon during the initial vegetative stage	0.20, 0.20, 0.20	Calibration parameter
Ar_{v1}	Initial allocation fraction for root carbon during the initial vegetative stage	0.36, 0.30, 0.30	Calibration parameter
Al_{v2}	Initial allocation fraction for leaf carbon during the normal vegetative stage	0.20, 0.30, 0.30	Calibration parameter
As_{v2}	Initial allocation fraction for stem carbon during the normal vegetative stage	0.60, 0.50, 0.60	Calibration parameter
Ar_{v2}	Initial allocation fraction for root carbon during the normal vegetative stage	0.20, 0.20, 0.10	Calibration parameter
Arh_r_{v2}	Initial reallocation fraction from rhizome to root during the normal vegetative stage in Eq. A8	0.30, 0.30, 0.30	Calibration parameter

Table 8 (continued)

Symbol	Definition	Values[a]	Source
Al_{r1}	Initial allocation fraction for leaf carbon during the initial reproductive stage	0, 0, 0	Calibration parameter
As_{r1}	Initial allocation fraction for stem carbon during the initial reproductive stage	0,15, 0.10, 0.10	Calibration parameter
Ap_{r1}	Initial allocation fraction for carbon in production pool during the initial reproductive stage	0.20, 0.40, 0.40	Calibration parameter
Ar_{r1}	Initial allocation fraction for root carbon during the initial reproductive stage	0.65, 0.50, 0.50	Calibration parameter
Arh_r_{r1}	Initial reallocation fraction from rhizome to root during the initial reproductive stage in Eq. A8	0.50, 0.50, 0.50	Calibration parameter
Al_{r2}	Initial allocation fraction for leaf carbon during the post reproductive stage	0, 0, 0	Calibration parameter
As_{r2}	Initial allocation fraction for stem carbon during the post reproductive stage	0, 0, 0	Calibration parameter
Ap_{r2}	Initial allocation fraction for carbon in production pool during the post reproductive stage	0, 0.4, 0.4	Calibration parameter
Ar_{r2}	Initial allocation fraction for root carbon during the post reproductive stage	1.0, 0.6, 0.6	Calibration parameter
Arh_r_{r2}	Initial reallocation fraction from rhizome to root during the post reproductive stage in Eq. A8	0.50,0.50,0.50	Calibration parameter
SLA_0	Specific leaf area	0.028, 0.03, 0.03 [m^2 g^{-1}]	[47]
V_{cmax25}	Maximum carboxylation rate at the reference temperature of 25 before N recycling adjustment	58, 38, 45 [μmol m^{-2} s^{-1}]	[46, 47, 67]
m	The slope of regressing stomatal conductance on carbon assimilation in Ball-Berry equation	8, 3, 3	Calibrated parameter
b	Minimum stomatal conductance in Ball-Berry equation	0.03, 0.03, 0.03 [mol m^{-2} s^{-1}]	Calibrated parameter
Rw_{max}	Maximum death rate of green leaves due to drought in leaves senescence simulation	0.035, 0.03, 0.035	Calibration parameter
T_{cold}	Cold temperature threshold for cold-induced death of green leaves	283, 285, 285 [K]	[8, 40, 64]
kl_1	Remove fraction of previous produced leaf litter in leaves senescence simulation	1.0	Calibration parameter
kl_2	Remove fraction of new produced leaf litter in leaves senescence simulation	0.91, 1.0, 1.0	Calibration parameter
rlt_{leaf}	Leaf turnover rate	0.78, 0.68, 0.68 [year]	[47]
rlt_{stem}	Stem turnover rate	1.0, 1.0, 1.0 [year]	
rlt_{root}	Root turnover rate	6.0, 6.0, 6.0[year]	
$rlt_{rhizome}$	Rhizome turnover rate	10.0, 10.0, 10.0 [year]	[68]
RS_{min}	Minimum root: shoot ratio of crop	0.19, 0.17, 0.17	[51]
CN_{leaf}	C:N ratio of leaf	61.5, 35, 35	[69]
CN_{stem}	C:N ratio of stem	112, 112, 112	[69]
$CN_{rhizome}$	C:N ratio of rhizome	65.6, 63, 63	Calculated based on [48]
CN_{root}	C:N ratio of root	112, 138, 138	Calculated based on [48]
k_{kill}	Parameter in Eq. A11	0.06, 0.01, 0.26	Calculated based on [13, 40, 42]
m_{kill}	Parameter in Eq. A11	−0.03, −0.10, −0.04	
R_{cyc}	N recycling rate per unit of Carbon	0.03, 0.01, 0.01 [kg N/kg C]	Calculated based on [43]

[a] The dash sign (−) represent that the parameter value is not needed for the specific bioenergy crop

Table 9 Additional ISAM model equations used in this study

Function		Equations
Heat requirement for flowering	$\text{GDD}_{v1}=\text{maximum } (900, 454\ln(\text{Latitude})-726)$	Eq. A1
Soil water availability	$\text{Wa}_i = \left(\frac{\theta t-\theta_c}{\theta_o-\theta_c}\right)\left(\frac{\varphi-f_c}{\varphi}\right)$	Eq. A2
Carbon storage in seed during its germination	$C_{\text{storage}}=C_{\text{seed}}\times(1+1.5\times\theta_H\times\theta_T)$	Eq. A3
	$\begin{cases} \theta_H = \psi-\psi_b & if \ \psi > \psi_b \\ \theta_H = 0 & if \ \psi\leq\psi_b \end{cases}$	Eq. A4
	$\begin{cases} \theta_T = T-T_{\text{base\_g}} \ if \ T_{\text{base\_g}} < T < T_{\text{opt\_g}} \\ \theta_T = \left(T_{\text{opt\_g}}-T_{\text{base\_g}}\right)(1-\frac{\left(T-T_{\text{opt\_g}}\right)}{\left(T_{\text{max\_g}}-T_{\text{opt\_g}}\right)}) \ if \ T_{\text{opt\_g}} < T < T_{\text{max\_g}} \end{cases}$	Eq. A5
Carbon allocation	The carbon allocation during seed germination of switchgrass in the planting year $\begin{cases} C_{\text{leaf}_i} = C_{\text{leaf}_{i-1}} + C_{\text{storage}} \times Al_{e1} \\ C_{\text{root}_i} = C_{\text{root}_{i-1}} + C_{\text{storage}} \times Ar_{e1} \end{cases}$	Eq. A6
	The carbon allocation during the emergence period	Eq. A7
	$\begin{cases} C_{\text{leaf}_i} = C_{\text{leaf}_{i-1}} + C_{\text{rhizome}_i} \times Ah_e \times Al_{e2} \\ C_{\text{stem}_i} = C_{\text{stem}_{i-1}} + C_{\text{rhizome}_i} \times Ah_e \times As_{e2} \\ C_{\text{rhizome}_i} = C_{\text{rhizome}_{i-1}} + C_{\text{rhizome}_i} \times Ah_e \\ C_{\text{root}_i} = C_{\text{root}_{i-1}} + C_{\text{rhizome}_i} \times Ah_e \times Ar_{e2} \end{cases}$	
	The carbon allocation during the initial and post reproductive stages $\begin{cases} C_{\text{root}_i} = C_{\text{root}_{i-1}} + C_{\text{root}_i} \times Ar \times Arh\_r \times (1-\text{Wa}) \\ C_{\text{rhizome}_i} = C_{\text{rhizome}_{i-1}} + C_{\text{root}_i} \times Ar \times (1-Arh\_r) \times \text{Wa} \end{cases}$	Eq. A8
Spring frost damage	The mortality of rhizome, root, leaf, and stem	Eq. A9
	$\begin{cases} L_{\text{leaf}_i} = C_{\text{leaf}_i} \times F_{\text{frost}} \\ L_{\text{stem}_i} = C_{\text{stem}_i} \times F_{\text{frost}} \\ L_{\text{root}_i} = C_{\text{root}_i} \times F_{\text{frost}} \\ L_{\text{rhizome}_i} = C_{\text{rhizome}_i} \times F_{\text{frost}} \end{cases}$	
	The frost factor for the mortality of rhizome, root, leaf, and stem	Eq. A10
	$\begin{cases} F_{\text{frost}} = \frac{T_{\text{frost}}-T_{\text{min3}}}{9} & if \ (T_{\text{frost}}-T_{\text{min3}})\leq 9 \\ F_{\text{frost}} = 1 & if \ (T_{\text{frost}}-T_{\text{min3}}) > 9 \end{cases}$	
Over-winter injury	The fraction of the rhizome mortality due to over-winter injury	Eq. A11
	$F_{\text{over\_winter}} = \begin{cases} \min\left(1.0, \left(k_{\text{kill}}e^{\left(m_{\text{kill}}\times\left(T_{\text{avg\_min}}-273.16\right)\right)}\right)\right) & if \ T_{\text{avg\_min}}\leq T_{\text{frost}} \\ 0 & if \ T_{\text{avg\_min}} > T_{\text{frost}} \end{cases}$	
Effect of photoperiod on SLA	$\begin{cases} \text{SLA} = \text{SLA}_0 \times \left(1-0.05\times\left(14-L_{day}\right)\right) & \text{For Miscanthus and Cave-in-Rock} \\ \text{SLA} = \text{SLA}_0 \times \left(1-0.05\times\left(L_{\text{day}}-12\right)\right) & \text{For Alamo} \end{cases}$	Eq. A12

Table 10 The location (latitude and longitude) and climate (annual mean temperature and accumulated precipitation) and soil characteristics of data sites used for model evaluation

Site ID	Site	State	Latitude (°)	Longitude (°)	Soil type	Plant hardiness zone	Annual mean temperature ( )	Annual total precipitation (mm)	Plot size (m²), replicated number	Reference
M1	Mead	NE	41.17	−96.47	Sandy Loam	5a	9	874	100, 12	[37]
M2	Adelphia	NJ	40.23	−74.25	Sandy loam	7a	12	1,167	100, 12	[37]
M3	Champaign	IL	40.03	−88.23	Flanagan silt loam	5b	10.7	1,041	100, 12	[37]
M4	Troy	KS	39.77	−95.20	Kennebec silt loam	6a	12.0	973	65, 4	[11]
M5	Manhattan	KS	39.18	−96.58	Iwan, Kennebec and Kahola silt loam	6a	12.0	943	65, 4	[11]
M6	Elsberry	MO	39.16	−90.79	Menfro silt loam	6a	13.0	972	20, 4	[32]
M7	Columbia	MO	38.89	−92.19	Mexico silt loam	6a	13.2	1,025	20, 4	[32]
M8	Lexington	KY	38.13	−84.50	Silt loam	6a	12.7	1,181	100, 12	[37]
M9	Mt. Vernon	MO	37.07	−93.81	Gerald silt loam	6a	14.2	1,171	100, 12	[37]

Table 10 (continued)

Site ID	Site	State	Latitude (°)	Longitude (°)	Soil type	Plant hardiness zone	Annual mean temperature ( )	Annual total precipitation (mm)	Plot size (m²), replicated number	Reference
M10	Stillwater	OK	36.12	−96.05	Kirkland silt loam	7a	16.7	932	20, 4	[32]
M11	Fayetteville	AR	36.09	−94.11	Pickwick gravely loam	6b	15.1	1,169	20, 4	[32]
M12	Booneville	AR	35.08	−93.98	Leadvale silt loam	7b	16.9	1,197	-, 4	[70]
M13	Nacogdoches	TX	31.50	−94.60	Attoyac fine sandy loam	8b	20.4	1,229	20, 4	[32]
M14	Gainesville	FL	29.65	−82.33	Urban land	9a	21.7	1,271		[71]
M15	Kingsville	TX	27.54	−97.85	Cranell sandy clay loam	9a	23.3	736	20, 4	[32]
M16	Ona	FL	27.48	−81.92	Pomona fine sand	9b	21.9	1,167	–	[71]
M17	Belle Glade	FL	26.68	−80.67	Terra Ceia muck	10a	24.7	1,188	–	[71]
C1	Dickinson	ND	46.88	−102.8	Farnuf fine sandy loam	4a	8.7	326	8.5, 4	[72]
C2	Mandan	ND	46.80	−100.92	Parshall fine sandy loam	4a	8.0	314	8.5, 4	[72]
C3	Brookings	SD	44.02	−97.09	Omega loamy sand	4b	8.2	608	2.9, 4	[73]
C4	Arlington	WI	43.33	−89.38	Plano silt loam	4b	8.5	911	4.8, 5	[73]
C5	Dekalb	IL	41.85	−88.85	Flangan silt loam	5b	10.9	821	100, 4	[14]
C6	Champaign	IL	40.08	−88.23	Flanagan silt loam	5b	12	1,021	100, 4	[47]
C7	Orr	IL	39.81	−90.82	Clarksdale silt	5b	12.9	1,028	100, 4	[14]
C8	Morgantown	WV	39.62	−79.95	Dormont silt loam	6b	11.9	1,068	15-20, 1	[55, 74]
C9	Elsberry	MO	39.16	−90.79	Menfro silt loam	6a	13.0	972	20, 4	[32]
C10	Brownstown	IL	38.95	−88.96	Cisne silt loam	6a	13.9	1,079	100, 4	[14]
C11	Columbia	MO	38.89	−92.19	Mexico silt loam	6a	13.2	1,025	20, 4	[32]
C12	Fairfield	IL	38.35	−88.35	Cisne silt loam	6a	14.3	1,145	100, 4	[14]
C13	Dixon Spring	IL	37.45	−88.67	Granstburg silt loam	6b	13.8	1,150	100, 4	[3]
C14	Princeton	KY	37.10	−87.82	Tilsit series	6b	15.1	1,261	20, 4	[55, 74]
C15	Mr. Vernon	MO	37.07	−93.81	Gerald silt loam	6a	14.2	1,171	20, 4	[32]
C16	Stillwater	OK	36.12	−96.05	Kirkland silt loam	7a	16.7	932	20, 4	[32]
C17	Fayetteville	AR	36.09	−94.11	Pickwick gravely loam	6b	15.1	1,169	20, 4	[32]
C18	Knoxville	TN	35.88	−83.95	Etowah clay loam	7a	14.0	1,267	15–20, 1	[55, 74]
C19	Raleigh	NC	35.72	−78.67	Cecil sandy loam	7b	15.5	1,140	15–20, 1	[55, 74]
C20	Jackson	TN	35.62	−88.83	Deanburg silt loam	7a	15.5	1,335	15–20, 1	[55, 74]
C21	Chickasha	OK	35.03	−97.91	McLain silt loam	7a	16.0	798	18, 3	[75]
C22	Dallas	TX	32.97	−97.27	Houston black clay	8b	18.8	943	18,2	[76]
C23	Nacogdoches	TX	31.50	−94.60	Attoyac fine sandy loam	8b	20.4	1,229	20, 4	[32]
C24	Temple	TX	31.06	−97.22	Houston black clay	8b	21	895	18, 2	[76]
C25	College station	TX	30.60	−96.35	Weswood silt clay loam	8b	20.5	993	18, 2	[76]
C26	Beeville	TX	28.4	−97.7	Parrita sandy clay loam and a Coy clay	9a	21.2	783	12, 2	[76]
C27	Kingsville	TX	27.54	−97.85	Cranell sandy clay loam	9a	23.3	736	20, 4	[32]
C28	Weslaco	TX	26.22	−98.13	Hidalgo sandy clay loam	9b	24.5	645	20, 4	[32]
A1	Morgantown	WV	39.62	−79.95	Dormont silt loam	6b	11.9	1,068	15–20, 1	[55, 74]
A2	Elsberry	MO	39.16	−90.79	Menfro silt loam	6a	13.0	972	20, 4	[32]
A3	Columbia	MO	38.89	−92.19	Mexico silt loam	6a	13.2	1,025	20, 4	[32]
A4	Orange	VA	38.22	−78.12	Davidson clay	7a	13.2	1,101	15–20, 1	[55, 74]
A5	Blacksburg	VA	37.18	−80.42	Shottower loam	6b	11.3	937	15–20, 1	[55, 74]
A6	Princeton	KY	37.10	−87.82	Tilsit series	6b	15.1	1,261	15–20, 1	[55, 74]
A7	Mt. Vernon	MO	37.07	−93.81	Gerald silt loam	6a	14.2	1,171	20, 4	[32]
A8	Stillwater	OK	36.12	−96.05	Kirkland silt lam	7a	23.3	932	20, 4	[32]

Table 10 (continued)

Site ID	Site	State	Latitude (°)	Longitude (°)	Soil type	Plant hardiness zone	Annual mean temperature ( )	Annual total precipitation (mm)	Plot size (m²), replicated number	Reference
A9	Fayetteville	AR	36.09	−94.11	Pickwick gravely loam	6b	15.1	1,169	20, 4	[32]
A10	Knoxville	TN	35.88	−83.95	Etowah clay loam	7a	14.0	1,267	15–20, 1	[55, 74]
A11	Raleigh	NC	35.72	−78.67	Cecil sandy loam	7b	15.5	1,140	15–20, 1	[55, 74]
A12	Jackson	TN	35.62	−88.63	Deanburg silt loam	7a	15.5	1,335	15–20, 1	[55, 74]
A13	Hope	AR	33.67	−93.58	Bowie loam sandy loam	8a	18.9	1,285	18, 4	[38]
A14	Dallas	TX	32.97	−97.27	Houston black clay	8b	18.8	943	18, 2	[76]
A15	Stephenville	TX	32.22	−98.20	Windthorst fine sandy loam	8a	19.8	666	18, 4	[38]
A16	Nacogdoches	TX	31.50	−94.60	Attoyac fine sandy loam	8b	20.4	1,229	20, 4	[32]
A17	Temple	TX	31.06	−97.22	Houston Black clay	8b	21.0	895	18, 2	[76]
A18	Clinton	LA	30.85	−90.05	Dexter silt loam	8b	20.4	1,428	18, 4	[38]
A19	College station	TX	30.60	−96.35	Weswood silt clay loam	8b	20.5	993	18, 2	[76]
A20	Beeville	TX	28.40	−97.7	Parrita sandy clay loam and a Coy clay	9a	21.2	783	12, 2	[76]
A21	Kingsville	TX	27.54	−97.85	Cranell sandy clay loam	9a	23.3	736	20, 4	[32]
A22	Weslaco	TX	26.22	−98.13	Hidalgo sandy clay loam	9b	24.5	645	20, 4	[32]

The sign (−) in the table means this information about plots size/replicated numbers is not available

References

1. Schnepf R, Yacobucci BD (2013) Renewable fuel standard (RFS): overview and issues. Congr Res Serv Rep Congr R40155
2. Gunderson CA, Davis EB, Jager HI, West TO, Perlack RD, Brandt CC, Wullschleger SD, Baskaran LM, Wilkerson EG, Downing ME (2008) Exploring potential U.S. switchgrass production for cellulosic ethanol using empirical modeling approaches. Oak Ridge National Laboratory, Oak Ridge, TN, ORNL/TM 2007/183
3. Heaton EA, Dohleman FG, Long SP (2008) Meeting US biofuel goals with less land: the potential of Miscanthus. GCB Bioenergy 14: 2000–2014
4. Lewandowski I, Scurlock JMO, Lindvall E, Christou M (2003) The development and current status of perennial rhizomatous gasses as energy crops in the US and Europe. Biomass Bioenergy 25:335–361
5. Casler MD, Vogel KP, Taliagerro CM, Wynia RL (2004) Latitudinal adaptation of switchgrass populations. Crop Sci 44:293–303
6. USDA, Plant Hardiness Zone Map (2012) Agricultural Research Service, U.S. Department of Agriculture. http://planthardiness.ars.usda.gov. Accessed 1 May 2013
7. Casler MD (2012) Switchgrass breeding, genetics, and genomics. In: Monti A (ed) Switchgrass, green energy and technology. Springer, London
8. Parrish DJ, Fike JH (2005) The biology and agronomy of switchgrass for biofuels. Plant Sci 24:423–459
9. Jager H, Baskaran LM, Brandt CC, Davis EB, Gunderson CA, Wullschleger SD (2010) Empirical geographic modeling of switchgrass yields in the United States. GCB Bioenergy 2:248–257
10. Nair SS, Kang S, Zhang X, Miguez FE, Izaurralde RC, Post WM, Dietze MC, Lynd LR, Wullschleger SD (2012) Bioenergy crop models: descriptions, data requirements, and future challenges. GCB Bioenergy 4(6):620–633
11. Propheter JL, Staggenborg S (2010) Performance of annual and perennial biofuel crops: nutrient removal during the first 2 years. Agron J 102:798–805
12. Behrman KD, Kiniry JR, Winchell M, Juenger TE, Keitt TH (2013) Spatial forecasting of switchgrass productivity under current and future climate change scenarios. Ecol Appl 23(1):73–85
13. Clifton-Brown JC, Neilson BM, Lewandowski I, Jones MB (2000) The modeled productivity of Miscanthus×giganteus (GREEF et DEU) in Ireland. Ind Crop Prod 12:97–109
14. Jain AK, Khanna M, Erickson M, Huang H (2010) An integrated biogeochemical and economic analysis of bioenergy crops in the Midwestern United States. GCB Bioenergy 2: 217–234
15. Hastings A, Clifton-Brown WJM, Mitchell CP, Smith P (2009) The development of MISCANFOR, a new Miscanthus crop growth model: towards more robust yield predictions under different climatic and soil conditions. GCB Bioenergy 1:154–170
16. Thomson AM, Izarrualde RC, West TO, Parrish DJ, Tyler DD, Williams JR (2009) Simulation potential switchgrass production in the United States. Pacific Northwest National Laboratory, Richland, WA, PNNL-19072
17. Miguez FE, Maughan M, Bollero GA, Long SP (2012) Modeling spatial and dynamic variation in growth, yield and yield stability of the bioenergy crops Miscanthus×giganteus and Panicum virgatum across the conterminous USA. GCB Bioenergy. doi:10.1111/j.1757-1707.2011.01150.x
18. VanLoocke A, Twine TE, Zeri M, Bernacchi CJ (2012) A regional comparison of water use efficiency for miscanthus, switchgrass and maize. Agric For Meteorol 164:82–95
19. Di Vittorio AV, Andersen RS, White JD, Miller NL, Running SW (2010) Development and optimization of an Agro-BGC ecosystem model for C4 perennial grasses. Ecol Model 221: 2038–2053
20. Zhuang Q, Qin Z, Chen M (2013) Biofuel, land and water: maize, switchgrass or Miscanthus? Environ Res Lett. doi:10.1088/1748-9326/8/1/015020
21. Barman R, Jain AK, Liang M (2013) Climate-driven uncertainties in terrestrial gross primary production: a site-level to global scale analysis. Glob Chang Biol. doi:10.1111/gcb.12474

22. Barman R, Jain AK, Liang M (2013) Climate-driven uncertainties in terrestrial energy and water fluxes: a site-level to global scale analysis. Glob Chang Biol. doi:10.1111/gcb.12473

23. El-Masri B, Jain AK, Barman R, Meiyappan P, Song Y, Liang M (2013) Carbon dynamics in the Amazonian basin: integration of eddy covariance and ecophysiological data with a land surface model. Agric For Meteorol. doi:10.1016/j.agrformet.2013.03.011

24. Song Y, Jain AK, Mclsaac GF (2013) Implementation of dynamic crop growth processes into a land surface model: evaluation of energy, water and carbon fluxes under corn and soybean rotation. Biogeosciences 10:8039–8066

25. Yang X, Witting V, Jain AK, Post WM (2009) Integration of nitrogen cycle dynamics into the integrated science assessment model for the study of terrestrial ecosystem responses to global change. Glob Biogeochem Cybern 23:GB4029. doi:10.1029/2009GB003474

26. Dai Y, Dickinson RE, Wang YP (2004) A two-big-leaf model for canopy temperature, photo- synthesis, and stomatal conductance. J Clim 17:2281–2299

27. Oleson KW, Niu G, Yang Z, Lawrence DM, Thornton PE, Lawrence PJ, Stöckli R, Dickinson RE, Bonan GB, Levis S, Dai A, Qian T (2008) Improvements to the community land model and their impact on the hydrological cycle. J Geophys Res 113:G01021. doi:10.1029/2007JG000563

28. Heaton EA, Boersma N, Caveny JD, Voigt TB, Dohleman FG (2014) Miscanthus (Miscanthus × giganteus) for biofuel production. http://www.extension.org/pages-/26625/miscanthus-miscanthus-x-giganteus-for-biofuel-production#.U4p41i9RFhE. Accessed 17 May 2014

29. Evers GW, Parsons MJ (2003) Soil type and moisture level influence on Alamo switchgrass emergence and seedling growth. Crop Sci 43:288–294

30. Zub HW, Brancourt-hulmel M (2010) Agronomic and physiological performances of different species of Miscanthus, a major energy. A review. Agron Sustain Dev 30:201–214

31. White MA, Thornton PE, Running SW (1997) A continental phenology model for monitoring vegetation responses to interannual climatic variability. Glob Biogeochem Cybern 11(2):217–234

32. Kiniry JR, Anderson LC, Johnson MVV, Behrman KD, Brakie M, Burner D et al (2013) Perennial biomass grasses and the Mason-Dixon line: comparative productivity across latitudes in the southern great plains. Bioenerg Res 6:276–291

33. Jensen E, Farrar K, Thomas-Jones S, Hastings A, Donnison I, Clifton-Brown J (2011) Characterization of flowering time diversity in Miscanthus species. GCB Bioenergy 3:387–400

34. Van Esbroeck GA, Hussey MA, Sanderson MA (2003) Variation between Alamo and Cave-in-Rock switchgrass in response to photoperiod extension. Crop Sci 43:639–643

35. Zegada-Lizarazu W, Wullschleger SD, Nair SS, Monti A (2012) Chapter 3 crop physiology. In: Monti A (ed) Switchgrass: a valuable biomass crop for energy. Springer, London, pp 55–86

36. Casler MD, Vogel KP, Taliaferro CM, Ehlke NJ, Berdahl JD, Brummer EC et al (2007) Latitudinal and longitudinal adaptation of switchgrass populations. Crop Sci 47:2249–2260

37. Maughan M, Bollero G, Lee DK, Darmody R, Bonos S, Cortese L, Murphy J, Gaussoin R, Sousek M, Williams D, Williams L, Miguez F, Voigt T (2012) Miscanthus × giganteus productivity: the effects of management in different environments. GCB Bioenergy 4:253–265

38. Cassida KA, Muir JP, Hussey MA, Read JC, Venuto BC, Ocumpaugh WR (2005) Biomass yield and stand characteristics of switchgrass in south Central U.S. environments. Crop Sci 45:673–681

39. Moser LE, Vogel KP (1995) Switchgrass, big bluestem, and indiangrass. In: Barnes RF et al (eds) Forages, an introduction to grassland agriculture, vol 1, 5th edn. Iowa State University Press, Ames, pp 409–421

40. Heaton EA, Dohleman FG, Miguez AF, Juvik JA, Lozovaya V, Widholm J, Zabotina OA, Mcisaac FG, David MB, Voigt TB, Boersma NN, Long SP (2010) Miscanthus: a promising biomass crop. Adv Bot Res 56:76–92

41. Roman ES, Murphy SD, Swanton CJ (2000) Simulation of chenopodium album seedling emergence. Weed Sci 48:217–224

42. Lemus R, Brummer EC, Moore KJ, Molstad NE, Burras CL, Barker MF (2002) Biomass yield and quality of 20 switchgrass populations in southern Iowa, USA. Biomass Bioenergy 23:433–442

43. Heaton EA, Dohleman FG, Long SP (2009) Seasonal nitrogen dynamics of Miscanthus × giganteus and Panicum virgatum. GCB Bioenergy 1:297–307

44. Mitchell KE, Lohmann D, Houser PR, Wood EF, Schaake JC, Robock A, Cosgrove BA, Sheffleld J, Duan Q, Luo L, Higgins RW, Pinker RT, Tarpley JD, Lettenmaier DP, Marshall CH, Entin JK, Pan M, Shi W, Koren V, Meng J, Ramsay BH, Balley AA (2004) The multi-institution North American land data assimilation system (NLDAS): utilizing multiple GCIP products and partners in a continental distributed hydrological modeling system. J Geophys Res. doi:10.1029/2003JD003823, D07S90

45. Soil Survey Staff, Natural Resources Conservations Service, United States Department of Agriculture. U.S. general soil map (STATSGO2). http://soildatamart.nrcs.usda.gov. Accessed 13 August 2013

46. Dohleman FG, Long SP (2009) More productive than maize in the midwest: how does Miscanthus do it? Plant Physiol 150:2104–2115

47. Dohleman FG, Heaton EA, Leakey ADB, Long SP (2009) Does greater leaf-level photosynthesis explain the larger solar energy conversion efficiency of Miscanthus relative to switchgrass? Plant Physiol 32:1525–1537

48. Dohleman FG, Heaton EA, Arundale RA, Long SP (2012) Seasonal dynamics of above- and below-ground biomass and nitrogen partitioning in Miscanthus × giganteus and Panicum virgatum across three growing seasons. GCB Bioenergy 4:534–544

49. Kiniry JR, Tischler CR, Van Esbroeck GA (1999) Radiation use efficiency and leaf CO_2 exchange for diverse C_4 grasses. Biomass Bioenergy 17:95–112

50. Willmott CJ, Robeson SM, Matsuura K (2012) A refined index of model performance. Int J Climatol 32:2088–2094

51. Barney JN, Mann JJ, Kyser GB, Blumwald E, Deynze AV, DiTomaso JM (2009) Tolerance of switchgrass to extreme soil moisture stress: ecological implications. Plant Sci. doi:10.1016/j.plantsci.2009.09.003

52. Moriasi DN, Arnold JG, Van Liew MW, Bingner RL, Harmel RD, ;Veith TL (2007) Model evaluation guidelines for systematic quantification of accuracy in watershed simulations. ASABE 50(3):885–900

53. Dohleman FG (2009) Seasonal dynamics of productivity and photosynthesis of three biofuel feedstocks: field comparisons of Miscanthus × giganteus, Panicum virgatum and Zea mays. Dissertation, University of Illinois at Urbana-Champaign, IL

54. Parrish DJ, Wolf DD, Fike JH, Daniels WL (2003) Switchgrass as a biofuels crop for the upper Southeast: variety trials and cultural improvements, Final report for 1997 to 2001. Oak Ridge National Laboratory, Oak Ridge, TN, ORNL/SUB-03019XSY163/01

55. Fike JH, Parrish DJ, Wolf DD, Balasko JA, Green JT Jr, Rasnake M, Reynolds JH (2006) Switchgrass production for the upper southeastern USA: influence of cultivar and cutting frequency on biomass yields. Biomass Bioenergy 30:207–213

56. Schmer MR, Mitchell RB, Vogel KP, Schacht WH, Marx DB (2009) Spatial and temporal effects on switchgrass stands and yield in the Great Plains. Bioenerg Res. doi:10.1007/s12155-009-9045-y

57. Blackmore S, Godwin RJ, Fountas S (2003) The analysis of spatial and temporal trends in yield map data over 6 years. Biosyst Eng 84(4):455–466

58. Pyter R, Voigt T, Heaton E, Dohleman F, Long SP (2007) Growing giant Miscanthus in Illinois. University of Illinois Extension, Urbana-Champaign

59. Rinehart L (2006) Switchgrass as a bioenergy crop. National sustainable agriculture information service. https://attra.ncat.org/attra-pub/summaries/summary.php?pub=311. Accessed 5 August 2013

60. Lee DK, Parrish AS, Voigt TB (2014) Switchgrass and giant Miscanthus agronomy. In: Shastri YA et al (eds) Engineering and biomass feedstock production and provision. Spring, New York, pp 37–59

61. Gibbons JD, Chakraborti S (2011) Nonparametric statistical inference, 5th edn. Chapman & Hall/CRC Press, Taylor & Francis Group, Boca Raton

62. Mclsaac GF, David MB, Mitchell CA (2010) Miscanthus and switchgrass production in central Illinois: impacts on hydrology and inorganic nitrogen leaching. J Environ Qual 39:1790–1799

63. Pennington D (2013) Bioenergy crops for Michigan and the Upper Midwest. http://cropwatch.unl.edu/bioenergy/forums. Assessed 10 May 2013

64. Sanderson MA, Wolf DD (1995) Morphological development of switchgrass in diverse environments. Agron J 87:908–915

65. USDA, NRCS (2013) The PLANTS Database, National plant data team, Greenboro, http://plants.usda.gov. Accessed 13 August 2013

66. Weng JH, Ueng RG (1997) Effect of temperature on photosynthesis of Miscanthus clones collected from different elevations. Photosynthetica 34(2):307–311

67. Wullschleger SD, Sanderson MA, McLaughlin SB, Biradar DP, Rayburn AL (1996) Photosynthetic rates and ploidy levels among populations of switchgrass. Crop Sci 36:306–312

68. Tufekcioglu A, Raich JW, Isenhart TM, Schultz RC (2003) Biomass, carbon and nitrogen dynamics of multi-species riparian buffers within an agricultural watershed in Iowa. USA Agrofor Syst 57:187–198

69. Johnson JMF, Barbour NW, Weyers SL (2007) Chemical composition of crop biomass impacts its decomposition. Soil Biol Biochem 71:155–162

70. Burner DM, Tew TL, Harvey JJ, Belesky DP (2009) Dry matter partitioning and quality of Miscanthus, Panicum, and Saccharum genotypes in Arkansas, USA. Biomass Bioenergy 33:610–619

71. Sollenberger LE, Erickson J, Vendramini J, Gilbert R, Soikiew A, Na C, Fedenko J (2010) Water-use efficiency and feedstock composition of candidate bioenergy grasses in Florida. Florida Energy Systems Consortium, pp 251–256, http://www.floridaenergy.ufl.edu/wp-content/uploads/Sollenberger.pdf. Accessed 13 August 2013

72. Berdahl JD, Frank AB, Krupinsky JM, Carr PM, Hanson JD, Johnson HA (2005) Biomass yield, phenology, and survival of diverse switchgrass cultivars and experimental strains in western North Dakota. Agron J 97:549–555

73. Casler MD, Boe AR (2003) Cultivar×environment interactions in switchgrass. Crop Sci 43:2226–2233

74. Fike JH, Parrish DJ, Wolf DD, Balasko JA, Green JT Jr, Rasnake M, Reynolds JH (2006) Long-term yield potential of switchgrass-for-biofuel systems. Biomass Bioenergy 30:198–206

75. Fuentes RG, Taliaferro CM (2002) Biomass yield stability of switchgrass cultivars. In: Janick J, Whipkey A (eds) Trends in new crops and new uses. ASHS Press, Alexandria, pp 276–282

76. Sanderson MA, Reed RL, Ocumpaugh WR, Hussey MA, Van Esbroeck G, Reed JC, Tischler CR, Hons FM (1999) Switchgrass cultivars and germplasm for biomass feedstock production in Texas. Bioresour Technol 67:209–219